PLATFORM FOR CALCIUM IMAGING, ISOLATION, AND CHARACTERIZATION IN PRIMARY COLON EPITHELIAL CELLS

Sebastian Mestril

A dissertation submitted to the faculty at the University of North Carolina at Chapel Hill in partial fulfillment of the requirements for the degree of Doctor of Philosophy in the Department of Biomedical Engineering in the School of Medicine.

Chapel Hill
2020

Approved by:

Shawn M. Gomez

Nancy L. Allbritton

Jeffrey M. MacDonald

Scott J. Bultman

Scott T. Magness

ABSTRACT

Sebastian Mestril: Platform for calcium imaging, isolation, and characterization in primary colon epithelial cells
(Under the direction of Dr. Nancy Allbritton)

The colonic epithelium, lining the innermost portion of the large intestine, is subjected to continued mechanical and chemical stress therefore requiring constant self-renewal. This renewal is supplied from the colon crypts which maintain and protect the intestinal stem cells in an undifferentiated state at the base. Through a multitude of growth factors, metabolites, gases, and extracellular matrix gradients along the colon crypt contributing to proliferation at the base and differentiation as cells migrate upwards. Recently, Ca^{2+} signaling has been identified as an integrator of multiple mitogenic signaling contributing to the regulation of stem-cell differentiation. These findings have yet to be fully explored with primary mammalian colon cells and face challenges in imaging 3D architecture such as organoids.

Chapter 2 addresses these challenges performing calcium imaging in 2D primary murine colon monolayers. Adopting imaging strategies originally developed for neuron calcium imaging, and image analysis pipeline was built capable of accurately isolating and extracting Ca^{2+} cell signals from the colon epithelium. Analyzing the isolate Ca^{2+} showed a correlation between higher frequencies and lower pulse width with proliferative cells, while broader oscillations occurring at a lower frequency were associated with differentiation. In Chapter 3 the impact of different growth factors is shown on the spatial temporal properties of the colon cell Ca^{2+} signals, demonstrating a similar relationship between higher frequency Ca^{2+} signals and

proliferation. Chapter 4 improves on the previous work introducing cells zones undergoing proliferation and differentiation, allowing for more targeted investigation in the Ca^{2+} signaling found in proliferative colon cells.

To my parents, Ruben & Ilona, who always supported me and pushed me to be my best

Erst die Arbeit, dann der Spass

To Jennifer & baby Tilly, my greatest support, biggest comfort and strongest motivation

ACKNOWLEDGEMENTS

There are many people that I would like to thank for the support and guidance throughout my graduate studies. I would first like to thank Nancy Allbritton, for offering me a position in the lab and always providing guidance throughout my graduate career. I would like to thank my committee members for all their input and joining when I changed projects, Shawn Gomez, Jeff MacDonald, Scott Bultman, and Scott Magness. A special thank you to Yuli Wang and Dulan Gunasekara, who were a tremendous help in research and troubleshooting.

I would like to thank all past and present members of the Allbritton group. Everyone made it a great place to work, and it was a pleasure working with all of you. A special thank you to the coffee and lunch crew, for my sanity would not have survived otherwise. Thank you to Sam Hinman, Jenny Huling, Angie Proctor, and Rayna Kim, for showing me how to be a better researcher while still having fun and always willing to lend a helping hand. Thank you to Johanna Dutton, for the coffee chats, valuable advice, and all the help transitioning to the colon team. A thank you to my desk buddy, Hannah Nowotarski, who always had my back and knew lunch should either bet at Al's or Heavenly Buffaloes. Under duress, I must thank Lauren Brown for helping with cell culture and introducing me to the term "bet".

Finally, I would like to thank my friends and family. A massive thank you to my parents, Ruben and Ilona Mestril, who have always encouraged my curiosity and creativity no matter my stubbornness. I will forever cherish the tales of ancient battles and will always think about air flow first when building an underground base. A loving thanks to my wife Jennifer, who after a wedding, two cats, and a baby Tilly has always been a source of support and I'm sure is excited

to start our next chapter together. To all my friends I made along the way, you have all been amazing and alone have made the degree worth it. Thank you to my Co-President Andy Brandt, it was a pleasure serving with you and am grateful to call you a friend. A special thank you to Peter & Nicole Bohlen, who have been a constant joy and amazing companions. Maybe someday the girls will take the lead in Pegs & Jokers, but probably not anytime soon.

TABLE OF CONTENTS

LIST OF TABLES

LIST OF FIGURES

LIST OF ABBREVIATIONS AND SYMBOLS

˚C	Degrees Celsius
β	Beta
µL	Microliter
µm	Micrometer
µM	Micromolar
γ	Gamma
2D	Two-Dimensional
3D	Three-Dimensional
A	Cell's Fluorescent Vector
ADMEM/F12	Advanced Dulbecco's Modified Eagle Medium/Nutrient Mixture F-12
ANOVA	Analysis of Variance
AM	Acetoxymethyl
AQuA	Astrocyte Quantitative Analysis
B	Background fluorescence
BMP	Bone Morphogenic Protein
BSA	Bovine Serum Albumin
C	Cell's Spatial Vector
Ca	Calcium
CaImAn	Calcium Image Analysis Toolkit
Caco-2	Adenocarcinoma of the colon (cells)
CalB	Calbindin
CalN	Calcineurin

CaM	Calmodulin
CCD	Charge-Coupled Device
CD	Crohn's Disease
CDI	*Clostridium Difficile* Infection
CNMF	Constrained Non-Negative Matrix Factorization
CNMF-E	Constrained Non-Negative Matrix Factorization Endoscope
CO_2	Carbon Dioxide
$CuSO_4$	Copper Sulfate
DI	Deionized
DM	Differentiation Media
DMSO	Dimethyl Sulfoxide
DNA	Deoxyribonucleic Acid
DTT	Dithiothreitol
E	Residual Fluorescence
ECM	Extracellular Matrix
EDC	1-ethyl-3-(3-dimethylaminopropyl) carbodiimide hydrochloride
EDTA	Ethylene-diamine tetra-acetic acid
EdU	(5-ethynyl-2-deoxyuridine)
EGF	Epidermal Growth Factor
EGFR	Epidermal Growth Factor Receptor
ENR-W	EGF, Noggin, RSpondin, Wnt
ER	Endoplasmic Reticulum
FBS	Fetal Bovine Serum

Fz	Frizzled
GCaMP	Calmodulin–M13 Fusion Protein
GECI	Genetically Encoded Calcium Indicator
GPa	Gigapascal
GPCR	G-Protein Coupled Receptor
GSK-β	Glycogen Synthesis Kinase 3 beta
GUI	Graphical User Interface
h	Hour
hr	Hour
HBSS	Hank's Balanced Salt Solution
HEPES	(4-(2-hydroxyethyl)-1-piperazineethanesulfonic acid)
IBD	Intestinal Bowel Disease
IF	Immunofluorescent
IL	Interleukin
InR	Insulin Receptor
IP3	Inositol Trisphosphate
IP3R	Inositol Trisphosphate Receptor
iPSC	Induced Pluripotent Stem Cell
ISC	Intestinal Stem Cell
JAK	Janus Kinase
JNK	c-Jun N-terminal kinases
KCl	Potassium Chloride
kDa	Kilodalton

kPa	Kilopascal
KRT20	Cytokeratin-20
L	Liter
Lgr5	Leucine rich repeat containing G-protein coupled receptor
L-WRN	L cells, Wnt, RSpondin, Noggin
mAb	Monoclonal Antibody
MES	2-(N-morpholino) ethanesulfoni acid
mg	Milligram
mGLuR5	Metabotropic Glutamate Receptor Type 5
min	Minute
Min1Pipe	Miniscope 1-Photon-Based Calcium Imaging Signal Extraction Pipeline
mL	Milliliter
mM	Millimolar
MSC	Mechanosensitive Channel
N_2	Nitrogen
NA	Numerical Aperture
NAC	N-acetyl Cysteine
NaCl	Sodium Chloride
NaN_3	Sodium Azide
NF-κB	Nuclear Factor kappa-light-chain-enhancer of activated B cells
NFAT	Nuclear Factor of Activate T-Cells
NHS	N-hydroxysuccinimide
nM	Nanomolar

OLFM4	Olfactomedin-4
PAA	Polyacrylic Acid
PBS	Phosphate Buffered Saline
PDMS	Polydimethylsiloxane
PEG	Polyethylene Glycol
PGMEA	Propylene Glycol Methyl Ether Acetate
PI	Propidium Iodide
PIP2	Phosphatidylinositol 4,5-bisphosphate
PKC	Protein Kinase C
PLC	Phospholipase C
PMCA	Plasma Membrane Ca^{2+} ATPase
PMT	Photomultiplier Tube
PN	Part Number
PNR	Peak to Noise Ratio
PSNR	Peak Signal to Noise Ratio
rcf	Relative Centrifugal Force
ROCC	Receptor-Operated Calcium Channel
ROI	Region of Interest
rpm	Revolutions per Minute
RSS	Residual Sum of Squares
RTK	Receptor Tyrosine Kinase
s	Second
SCFA	Short Chain Fatty Acid

sec	Second
SERCA	Sarco/Endoplasmic Reticulum Ca^{2+}-ATPase
SNR	Signal to Noise Ratio
STAT	Signal Transducer and Activator of Transcriptional Proteins
RTK	Receptor Tyrosine Kinase
TA	Transit Amplifying
TAZ	Transcriptional Co-Activator with PDC binding motif
TEER	Transepithelial Electrical Resistance
TGF-β	Transforming Growth Factor Beta
TJ	Tight Junction
TNF	Tumor Necrosis Factor
TRPV1	Transient Receptor Potential Cation Channel, Subfamily V, Member 1
UC	Ulcerative Colitis
UNC	University of North Carolina
UV	Ultraviolet
v/v	Volume per Volume
VGC	Voltage-Operated Channel
Wnt	Wingless:integration site
wt%	Percentage by mass
w/v	Weight by volume
YAP	Yes-Associate Protein 1

CHAPTER 1: INTRODUCTION

1.1 Ca^{2+} signaling

Ca^{2+} has been well established as a vital secondary messenger and is ubiquitous across cell types[1, 2]. The signaling toolkit of Ca^{2+} is capable of encoding information through the dynamic concentration of cytosolic Ca^{2+} and through its decoding influence multiple cellular processes in response to many chemical mechanical, and electrical inputs.

1.1.1 Signaling toolkit

Cells are required to maintain a cytosolic Ca^{2+} homeostasis (~0.1μM) due to toxicity and therefore sequester the Ca^{2+} ions into organelles or across the plasma membrane[2]. The activation of electrically-gated, mechanically-gates or receptor-operate channels can lead to the diffusion of Ca^{2+} down a concentration gradient into the cytosol[3, 4]. There are also G-protein-coupled receptors (GPCRs) and receptor tyro-sine kinase (RTKs) which through phospholipase C (PLC) activate inositol triphosphate receptors (IP3Rs) release the cells stores of Ca^{2+} from the endoplasmic reticulum (ER). Downstream of the elevated cytosolic Ca^{2+}, there exist many proteins with Ca^{2+} binding domains. This include Calmodulin (CaM) and calbindin (CalB), which can activate different kinases and phosphates including CaM kinase and calcineurin (CalN)[5–7].

1.1.2 Spatial-temporal characteristics of Ca^{2+} signaling

The different spatial-temporal characteristics of Ca^{2+} signaling can vary greatly throughout the cell. The initial release of Ca^{2+} into the cytosol can remain localized on the order of less than a micron as the result of a single membrane-bound channel source (Ca^{2+} blips or puffs), or completely fill the cell cytosol through the activation of multiple adjacent channels opening in concert (Ca^{2+} spikes)[1, 1, 8, 9]. Large Ca^{2+} signals are also capable of propagating to neighboring cells through gap-junction diffusion or paracrine signaling, resulting in a Ca^{2+} wave through multiple cells. The temporal dynamics of Ca^{2+} signaling can occur on the magnitude of multiple milliseconds to multiple minutes. Due to the cell's requirement of preventing toxic concentrations of Ca^{2+} and maintaining homeostasis, oscillations are naturally developed [10]. The dynamic nature of these signals has the added benefit of high information density through amplitude, frequency, shape, and basal concentration over a traditional static concentration. With this information density, Ca^{2+} is able to integrate many inputs signals and relay to many targets which is sometimes referred to as a bow-tie motif in biological systems[11, 12]. An example of information flow through the bow-tie motif is the targeting of either downstream transcription factor NFAT or NF-kB depending on decoding of Ca^{2+} oscillations (also known as a ratcheting mechanism)[13, 14].

1.2 Large intestinal epithelium

1.2.1 Large intestine structure and function

The large intestine, or large bowel, has three primary functions which are the absorption of water and electrolytes, the production and absorption of vitamins, and the removal of useless waste material from the body[15]. The large intestine wall is made up of multiple layers, which

moving outward are the mucosa, submucosa, muscular layer, and serosa. The exterior muscular layer and ceros aid in the austral contraction and mass movement motilities present within the colon. The inner mucosa layer is comprised of a lining epithelium, an underlying loose connective tissue called the lamina propria which provides vascular support, and a thin double layer of smooth muscles called the muscular mucosa for local movement of the mucosa[16]. In comparison with the small intestine epithelium, the large intestine does not have evaginations (villi) and instead has invaginations called crypts in which pluripotent stem cells reside[17].

1.2.2 Stem cell niche

The colonic epithelium, lining the innermost portion of the large intestine, is subjected to continuous mechanical stress and chemical gradients, resulting in a complete renewal of the tissue within 3 to 5 days in human, or 2 to 3 days in mice[18, 19]. This constant cell renewal originates from small invaginations within the colon epithelium, or crypts, containing multiple cell types but most importantly intestinal stem cells (ISCs)[20, 21]. At the base of the crypts, the ISCs remain in an undifferentiated state and are maintained through a multitude of growth factors, metabolites, gases, and extracellular matrix gradients. ISCs divide to produce transit amplifying (TA) cells which migrate upwards along the crypt axis and undergo a finite number of cells divisions before ultimately differentiating into absorptive or secretory cell lineages (e.g. goblet and enteroendocrine). In order to better understand these cell compartments multiple strategies have been employed to mimic the *in vivo* architecture and gradients.

A complex collection of gradients exists within the colon crypt stem cell niche, balancing proliferation and differentiation[22]. Key regulatory signals within the colon crypt include conical Wnt signaling, bone morphogenetic protein (BMP), and Notch signaling pathways. Wnt and Notch signaling is largest at the base of the colon crypt promoting ISC self-renewal[23].

Homeostatic Notch signaling results in progenitor cells predominately differentiating into absorptive cells but when decreased shift to secretory cell fates[24]. At the luminal end of the crypt, are elevated concentrations of BMP-2 and BMP-4 secreted by inter-crypt mesenchymal cells[25]. BMP signaling promotes differentiation through the Smad-mediated transcriptional repression of multiple signature genes that promote stemness[26]. The intestine is also host to microbiota, which produce a vast array of metabolites such as polyamines and short-chain fatty acids (SCFAs)[27–29]. The crypt structure decreases the exposure of these metabolites to ISCs and progenitors. A screen of 92 molecules showed butyrate, a product of the bacterial fermentation of dietary fiber, as a potent suppressor of proliferation even with Wnt signaling present[30]. The extracellular matrix surrounding the colon crypt exhibit gradients, aiding in the promotion of proliferation or differentiation of colon cells. Through the advancement of in vitro culture methods, 1.3 kPa of has been found as an optimal scaffold stiffness for the promotion of colon cell proliferation[31].

1.2.3 Ca^{2+} signaling in colon epithelium

Recent studies have determined Ca^{2+} to be a vital secondary messenger in the regulation of stem-cell activity within the colon crypt. Utilizing the *Drosophila* model for the study the metabotropic glutamate receptor mGluR5, Deng et al. found cytosolic Ca^{2+} signaling in intestinal epithelial cells acted as an integrator for multiple mitogenic signals impacting tissue homeostasis[32]. Under conditions of high nutrition or stress calcium oscillations became less frequent but with larger amplitudes and pulse widths leading to a higher cumulative concentration of Ca^{2+} within the cytosol. Inversely during times of starvation or homeostasis the Ca^{2+} pulses were stochastic and narrow in pulse width. Similar findings were demonstrated by Li et al. using the *Drosophila* model to the study the stretch-activated ion channel Piezo[4].

Consecutive mechanical stress applied to the gut activated the Piezo channel and allowed extracellular Ca^{2+} into the cytosol in large oscillations. The elevated cumulative cytosolic Ca^{2+} lead to higher cell differentiation and was inhibited with the silencing of certain key components of the calcium signaling pathway such as Stim and SERCA. These findings show Ca^{2+} as a signal integrator for the *Drosophila* ISCs of multiple mitogenic signals but has yet been reproduced in primary mammalian colon cells.

1.3 Ca^{2+} imaging and signal analysis

1.3.1 Ca^{2+} indicators

The current understanding of Ca^{2+} signals can be greatly attributed to fluorescent Ca^{2+} indicators and their continued improvement. The first of these fluorescent indicators was developed by Tsein et al., successfully synthesizing multiple organize Ca^{2+} indicators and creating a simplified loading technique in large intact cell populations[33–35]. These early dyes consisted of a Ca^{2+} chelating moiety conjugated to a fluorescence reporter and masked with an acetoxymethyl (AM) ester (quin-2, Rhod-1, -2, and Fluo-1, -2, -3). The now uncharged hydrophobic indicator is now freely capable of crossing the cell membrane, entering the cytosol. The AM groups are then cleaved through non-specific intercellular esterase, reverting the indicator back to a charge state and trapping it within the cell. At low concentrations of cytosolic Ca^{2+}, the conjugated fluorophore is quenched through photo-induced electron transfer. At elevated concentrations of cytosolic Ca^{2+}, this phenomenon is inhibited and the fluorescence increases. Certain indicators, known as ratiometric indicators, undergo a shift in spectral properties in response to the elevated Ca^{2+} and altering the optimum excitation or emission wavelength (fura-2 and indo-1)[33]. Ratiometric indicators provide a more detailed quantification

of the intracellular Ca^{2+} concentration but require more complex optics hardware, limited sample rate, and often require excitation by phytotoxic wavelengths[36]. In comparison, single wave indicators are easier to implement and are more broadly adopted in researching subcellular Ca^{2+} transients[37]. They also offer a substantial increase in fluorescence and can be normalized through the elevation of cytosolic Ca^{2+} concentration to saturation.

Genetically encoded calcium indicators (GECI) have also been developed in parallel for the improved cell target and imaging of complex *in vivo* tissue. GECI's remove the necessity of indicator loading and are capable of targeting specific cell populations[38–40]. This is particular useful in the calcium imaging of neuron populations for the study of network activity in live brains[41]. In comparison with organic Ca^{2+} indicators, GECIs are still limited in selection and in certain contexts have inferior performance in signal-to-noise ratio and sensitivity[37].

1.3.2 Neural calcium imaging

Neural research uses calcium imaging to gain a better understanding of how sensations and behavior are encoded in activity patterns of neural circuitry. To observe the neural activity calcium imaging is commonly utilized with one-photon or two-photon imaging in living mammalian brains[41, 42]. Technical advances in this field have led to improvements in the capacity and quality of neurons imaged, resulting in sometimes monitor activity of several thousand neurons[43]. Each of the neuron under study requires motion correction, associated area, spike deconvolution and most importantly quality control[44]. There exists a wide range of computational research addressing these different challenges and several packages exist combining them into a single calcium image analysis pipeline[45–47].

1.4 Overview of this dissertation

The work of this dissertation was focused on the development of a platform for the accurate imaging, capturing, and characterization of Ca^{2+} signals in primary murine colon epithelium. Chapter 2 outlines the initial identification of Ca^{2+} fluctuations in a self-renewing colon monolayer and the subsequent steps to isolate the cell signals for characterization. A final image analysis pipeline was constructed using MATLAB and calcium imaging software commonly used in neuron research. With a platform established, chapter 3 investigates the impact of different extracellular stimuli on the spatial-temporal characteristics of cellular Ca^{2+} oscillations. The different stimuli included growth factors, differentiation factors, dietary compounds, and extracellular stiffness. The work in chapter 4 improves upon the previous work, using a microdevice to compartmentalize actively proliferating cells through controlled availability of growth factors.

REFERENCES

1. Berridge MJ, Lipp P, Bootman MD. The versatility and universality of calcium signaling. Nature Reviews Molecular Cell Biology. 2000;1:11-21.

2. Clapham DE. Review Calcium Signaling. Cell. 2007;131:1047-1058.

3. Catterall WA. Voltage-gated calcium channels. Cold Spring Harbor perspectives in biology. 2011 Aug 1;3(8):a003947.

4. He L, Si G, Huang J, Samuel ADT, Perrimon N. Mechanical regulation of stem-cell differentiation by the stretch-activated Piezo channel. Nature. 2018

5. Yiu W, Science S, Series N, Jan N. Calmodulin Plays a Pivotal Role in Cellular Regulation Published by : American Association for the Advancement of Science Linked references are available on JSTOR for this article : Calmodulin Plays a Pivotal Role in Cellular Regulation. 2018;207:19-27.

6. Klee CB, Crouch TH, Krinks MH. Calcineurin: A calcium- and calmodulin-binding protein of the nervous system. Proceedings of the National Academy of Sciences of the United States of America. 1979;76:6270-6273.

7. Saucerman JJ, Bers DM. Calmodulin mediates differential sensitivity of CaMKII and calcineurin to local Ca2+ in cardiac myocytes. Biophysical Journal. 2008;95:4597-4612.

8. Wu Q, Brodskiy PA, Huizar F et al. In vivo relevance of intercellular calcium signaling in Drosophila wing development. 2017

9. Balaji R, Bielmeier C, Harz H et al. Calcium spikes, waves and oscillations in a large, patterned epithelial tissue. Scientific Reports. 2017;7:1-14.

10. Cheong R, Levchenko A. Oscillatory signaling processes: the how, the why and the where. Curr Opin Genet Dev. 2010;20:665-669.

11. Friedlander T, Mayo AE, Tlusty T, Alon U. Evolution of bow-tie architectures in biology. PLoS Comput Biol. 2015;11:e1004055.

12. Polouliakh N, Nock R, Nielsen F, Kitano H. G-protein coupled receptor signaling architecture of mammalian immune cells. PLoS One. 2009;4:e4189.

13. Cooling MT, Hunter P, Crampin EJ. Sensitivity of NFAT cycling to cytosolic calcium concentration: implications for hypertrophic signals in cardiac myocytes. Biophys J. 2009;96:2095-2104.

14. Dolmetsch RE, Xu K, Lewis RS. Calcium oscillations increase the efficiency and specificity of gene expression. Nature. 1998;392:933-936.

15. Edmonds CJ. Water and ionic transfer pathways of mammalian large intestine. Clinical Science. 1981;61:257-263.

16. Azzouz LL, Sharma S. Physiology, Large Intestine StatPearls [Internet]. StatPearls Publishing; 2019.

17. Grosse AS, Pressprich MF, Curley LB et al. Cell dynamics in fetal intestinal epithelium: Implications for intestinal growth and morphogenesis. Development. 2011;138:4423-4432.

18. Crossman MW, Hauft SM, Gordon JI. The mouse ileal lipid-binding protein gene: A model for studying axial patterning during gut morphogenesis. Journal of Cell Biology. 1994;126:1547-1564.

19. Potten CS, Kellett M, Roberts SA, Rew DA, Wilson GD. Measurement of in vivo proliferation in human colorectal mucosa using bromodeoxyuridine. Gut. 1992;33:71-78.

20. Barker N, van Es JH, Kuipers J et al. Identification of stem cells in small intestine and colon by marker gene Lgr5. Nature. 2007;449:1003-1007.

21. Sangiorgi E, Capecchi MR. Bmi1 is expressed in vivo in intestinal stem cells. Nat Genet. 2008;40:915-920.

22. Wang Y, Kim R, Hinman SS, Zwarycz B, Magness ST, Allbritton NL. Bioengineered Systems and Designer Matrices That Recapitulate the Intestinal Stem Cell Niche. Cmgh. 2018;5:440-453.e1.

23. Pinto D, Gregorieff A, Begthel H, Clevers H. Canonical Wnt signals are essential for homeostasis of the intestinal epithelium. Genes Dev. 2003;17:1709-1713.

24. VanDussen KL, Carulli AJ, Keeley TM et al. Notch signaling modulates proliferation and differentiation of intestinal crypt base columnar stem cells. Development. 2012;139:488-497.

25. Haramis APG. Erratum: De novo crypt formation and juvenile polyposis on BMP inhibition in mouse intestine (Science (March 12) (1684)). Science. 2004;304:1449.

26. Qi Z, Li Y, Zhao B et al. BMP restricts stemness of intestinal $Lgr5^{+}$ stem cells by directly suppressing their signature genes. Nat Commun. 2017;8:13824.

27. Qin J, Li R, Raes J et al. A human gut microbial gene catalogue established by metagenomic sequencing. Nature. 2010;464:59-65.

28. Matsumoto M, Kibe R, Ooga T et al. Impact of Intestinal Microbiota on Intestinal Luminal Metabolome. Scientific Reports. 2012;2

29. Sridharan GV, Choi K, Klemashevich C et al. Prediction and quantification of bioactive microbiota metabolites in the mouse gut. Nat Commun. 2014;5:5492.

30. Kaiko GE, Ryu SH, Koues OI et al. The Colonic Crypt Protects Stem Cells from Microbiota-Derived Metabolites. Cell. 2016;167:1137.

31. Gjorevski N, Sachs N, Manfrin A et al. Designer matrices for intestinal stem cell and organoid culture. Nature. 2016;539:560-564.

32. Deng H, Gerencser AA, Jasper H. Signal integration by Ca(2+) regulates intestinal stem-cell activity. Nature. 2015;528:212-217.

33. Grynkiewicz G, Poenie M, Tsien RY. A new generation of Ca2+ indicators with greatly improved fluorescence properties. Journal of Biological Chemistry. 1985;260:3440-3450.

34. Tsien RY. A non-disruptive technique for loading calcium buffers and indicators into cells. Nature. 1981;290:527-528.

35. Minta A, Kao JPY, Tsien RY. Fluorescent indicators for cytosolic calcium based on rhodamine and fluorescein chromophores. Journal of Biological Chemistry. 1989;264:8171-8178.

36. Hyrc KL, Minta A, Escamilla PR, Chan PP, Meshik XA, Goldberg MP. Synthesis and properties of Asante Calcium Red--a novel family of long excitation wavelength calcium indicators. Cell Calcium. 2013;54:320-333.

37. Lock JTDON, Behavior UOC, Irvine, CA, Parker I, Smith IFDON, Behavior UOC, Irvine, CA. A comparison of fluorescent Ca2+ indicators for imaging local Ca2+ signals in cultured cells. Cell Calcium. 2016;34:352-359.

38. Tian L, Hires SA, Mao T et al. Imaging neural activity in worms, flies and mice with improved GCaMP calcium indicators. Nature Methods. 2009;6:875-881.

39. Russell JT. Imaging calcium signals in vivo: A powerful tool in physiology and pharmacology. British Journal of Pharmacology. 2011;163:1605-1625.

40. Ni Q, Mehta S, Zhang J. Live-cell imaging of cell signaling using genetically encoded fluorescent reporters. FEBS Journal. 2018;285:203-219.

41. Göbel W, Helmchen F. In vivo calcium imaging of neural network function. Physiology (Bethesda). 2007;22:358-365.

42. Resendez SL, Stuber GD. In vivo Calcium Imaging to Illuminate Neurocircuit Activity Dynamics Underlying Naturalistic Behavior. Neuropsychopharmacology. 2015;40:238-239.

43. Grewe BF, Langer D, Kasper H, Kampa BM, Helmchen F. High-speed in vivo calcium imaging reveals neuronal network activity with near-millisecond precision. Nature Methods. 2010;7:399-405.

44. Stringer C, Pachitariu M. Computational processing of neural recordings from calcium imaging data. Current Opinion in Neurobiology. 2019;55:22-31.

45. Pachitariu M, Stringer C, Dipoppa M et al. Suite2p: beyond 10,000 neurons with standard two-photon microscopy. 2016

46. Jang MJ, Nam Y. NeuroCa: integrated framework for systematic analysis of spatiotemporal neuronal activity patterns from large-scale optical recording data. Neurophotonics. 2015;2:035003.

47. Lu J, Li C, Singh-Alvarado J et al. MIN1PIPE: A Miniscope 1-Photon-Based Calcium Imaging Signal Extraction Pipeline. Cell Rep. 2018;23:3673-3684.

CHAPTER 2: IDENTIFICATION AND CHARACTERIZATION OF INTRACELLULAR CA^{2+} SIGNALING IN MURINE COLON EPITHELIUM

2.1 Introduction

Ca^{2+} remains a ubiquitous intracellular messenger across all cell types and is involved in regulating many cellular processes including growth, death, differentiation, cytoskeletal mechanics, and protein secretion[1–4]. The ability for such versatility from a single cation resides in the information density that can be obtained from a dynamic signal. In comparison to a unidirectional signal such as an increase in extracellular [Ca^{2+}], bidirectional oscillations of cytoplasmic [Ca^{2+}] can encode information through frequency, amplitude, and cumulative concentration. The period of these oscillations can vary between a few milliseconds in excitable cells, cardiomyocytes for example[5], to a few seconds or minutes in non-excitable cells such as embryonic kidney cells[6]. Although all ranges of Ca^{2+} signaling remain vital to cellular upkeep, slower oscillations within epithelia cells have found to be crucial in tissue-level growth, renewal, and repair[7–9].

For improved understanding of cellular Ca^{2+} signaling and direct monitoring, multiple fluorescent indicators with improving optical technologies have been developed. The first developed by Tsein et al., successfully synthesizing multiple organic Ca^{2+} indicators (quin-2, Rhod-1, -2, and Fluo-1, -2, -3) and creating a simplified loading technique in large intact cell populations[10–12]. Masking the negatively charged carboxyl groups with acetoxymethyl (AM) ester results in an uncharged hydrophobic indicator now capable of crossing the cell membrane. Once within the cytosol the AM groups are cleaved through non-specific intracellular esterase,

reverting the indicator back to a charged state and trapped within the cell. Dependent on the indicators response to changing Ca^{2+} concentrations, they can be categorized as single wavelength or dual wavelength more commonly known as ratiometric. When a ratiometric indicator (fura-2 and indo-1) binds with a calcium ion either the optimum excitation or emission wavelength is altered, allowing a quantitative measurement of the Ca^{2+} as a ratio between the two states[11]. Although ratiometric indicators have the advantage of delivering quantitative data they require more complex optics hardware, limited image acquisition rate, and often require excitation by phototoxic wavelengths[13]. For more targeted loading in complex tissues, particularly *in vivo*, genetically encoded calcium indicators (GECIs) calcium sensitive proteins can be expressed in transgenic animals using specific promotors[14, 15]. The GECIs have the advantage of specific loading and the ability to perform long-term in vivo, yet are still limited in selection and in certain instances have inferior performance to traditional indicators in signal-to-noise ratio and sensitivity[16].

The ability to study the Ca^{2+} dynamics from fluorescent image data is possible with manual region of interest (ROI) selection but limited in throughput and has therefore led to the multiple automated and semi-automated computational tools. A large portion of these tools have stemmed from neuronal research pursuing better understanding of complex neural circuits through monitoring the firing of action potentials lasting a few hundred in milliseconds in sometimes 1,000 or more neurons in a single field of view[17]. In addition to the large amount of image data produced, isolating the action potentials requires motion correction for either multi-day imaging or live *in vivo* imaging, ROI isolation, spike deconvolution, and finally quality control[18]. Each of these hurdles have led to their own algorithmic solutions and several packages exist combining them into a full Ca^{2+} image analysis pipeline[19–21]. The most cited of these being

CNMF/CaImAn software package developed by the Flatiron Institute, combining piecewise rigid motion correction, non-negative matrix factorization, and sparse non-negative in a resource efficient package capable of running on most computers[22, 23]. The availability of efficient yet simple tools for Ca^{2+} measurement has becoming increasingly important not only in excitable cells but also for non-excitable cells such as epithelial tissue[24].

The colonic epithelium, lining the innermost portion of the large intestine, is subjected to continuous mechanical stress and chemical gradients, resulting in a complete renewal of the tissue within 3 to 5 days in human, or 2 to 3 days in mice[25, 26]. This constant cell renewal originates from small invaginations within the colon epithelium, or crypts, containing multiple cell types but most importantly intestinal stem cells (ISCs)[27, 28]. At the base of the crypts, the ISCs remain in an undifferentiated state and are maintained through a multitude of growth factors, metabolites, gases, and extracellular matrix gradients. ISCs divide to produce transit amplifying (TA) cells which migrate upwards along the crypt axis and undergo a finite number of cells divisions before ultimately differentiating into absorptive or secretory cell lineages (e.g. goblet and enteroendocrine). In order to better understand these cell compartments multiple strategies have been employed to mimic the *in vivo* architecture and gradients.

There have been multiple advancements in modeling the intestinal structural and mechanical properties, initially using immortalized cells such as Caco-2 cell lines. These devices have included micro-molded hydrogels for villi formation and micro-fluidic devices allowing for flow above and below the modeled epithelium[29, 30]. Although versatile, the carcinoma-derived models are limited in their modeling of the *in vivo* physiology including undefined DNA mutations and limited epithelial cell diversity[31]. Recent developments in cell culture have also allowed for the utilization of primary cells, derived directly from human or mouse subjects,

providing a more accurate equivalency to *in vivo* studies. Initially studied as organoids or monolayers, these primary cells are now being developed in complex 3D architectures for better imitation of *in vivo* physiology[32, 33].

Another promising platform for studying the gastrointestinal tract and Ca^{2+} signaling is the *Drosophila* intestine which also undergoes self-renewal mediated by small populations of stem cells. As an experimental model, the *Drosophila* benefits from relative genetic simplicity, short life span, and minimal upkeep. Utilizing the *Drosophila* model for the study the metabotropic glutamate receptor mGluR5, Deng et al. found cytosolic Ca^{2+} signaling in intestinal epithelial cells acted as an integrator for multiple mitogenic signals impacting tissue homeostasis. Under conditions of high nutrition or stress calcium oscillations became less frequent but with larger amplitudes and pulse widths leading to a higher cumulative concentration of Ca^{2+} within the cytosol. Inversely during times of starvation or homeostasis the Ca^{2+} pulses were stochastic and narrower in pulse width. These findings show Ca^{2+} as a signal integrator for the *Drosophila* ISCs but has yet been reproduced in primary mammalian colon cells.

Preliminary investigations have been made into Ca^{2+} signaling and ISC proliferation in primary mammalian colon cells. Murine colon organoids were loaded with Fura-2 and imaged by Yamazaki et al researching the Mg^{2+} transporter CNNM4, while human organoids and *ex vivo* 3D native colon crypts were imaged in a similar fashion by Lines et al studying calcium signaling in response to cholinergic signaling[34, 35]. Both studies provided promising insight into colon crypt Ca^{2+} signaling. The 3D cell models however, limit the accessible single cell information through traditional microscopy and the versatility in manipulating extracellular stimuli. A new system is required for more concentrated investigations on the role of Ca^{2+}

signaling in mammalian ISC proliferation. This system would require the ability to observe Ca^{2+} signaling at a single cell resolution and mimic the cell heterogeneity found in *in vivo* colon crypts.

In the current work, an image analysis pipeline adapted from neuronal research has been applied for the study of the calcium signaling within a self-renewing monolayer of primary colonic epithelial cells with single-cell resolution. Wang et al. developed a 2D self-renewing monolayer of primary murine colonic epithelial cells, providing a platform for single focal plane imaging of cells in culture[36]. This culture format, relying on a planar collagen hydrogel support, maintains all major cell types of the colonic epithelium, and thus was determined optimal for modeling the *in vivo* colon. Challenges in isolating fluorescent indicator-based calcium signals include high local background fluorescence and photo bleaching. To overcome these challenges, a pipeline was constructed from the Calcium Imaging Analysis (CaImAn) toolkit developed by the Flatiron institute[22, 37]. The toolkit was applied to create an image analysis pipeline and optimized based on performance specific to the calcium temporal stacks collected from colon cell patches. The constructed pipeline enabled the ability to accurately isolate signals, removing both global and localized fluorescence background while correcting for photobleaching of the calcium indicator. Performing calcium imaging on monolayers of colon epithelium provided a robust collection of Ca^{2+} signals, with a majority of features occurring within 72 hours of passage and then a significant decrease thereafter. Studying the spatial-temporal properties of the Ca^{2+} signals revealed an increase in period and decrease in frequency as the cells reached >80% confluency of the culture wells.

2.2 Materials and Methods

2.2.1 Materials

The following organic Ca^{2+}-dyes in acetoxymethyl (AM) ester form: Fluo-4 (Thermo Fisher Scientific, Waltham, MA) and Cal-520 (Abcam, Cambridge, MA). Dyes were reconstituted with dimethyl sulfoxide (DMSO) to a final concentration of 1 mM and stored, shielded from light, at -20 °C. DMSO, A83-01, and probenecid were obtained from Sigma-Aldrich Corp. (St. Louis, MO). Rat tail type I collagen, 6-well and 24-well polystyrene tissue culture dishes, and HEPES purchased from Corning (Corning, NY). Collagenase (type IV) was purchased from Worthington Biochemicals (Lakewood, NJ). Murine EGF was obtained from Peprotech (Rock Hill, NJ). Primocin purchased from InvivoGen (San Diego, CA). Y-27632 (A3008-200) purchased from ApexBio Technology (Houston, TX). L-WRN CRL-3276 cell line was purchased from ATCC (Manassas, VA). All other reagents purchased from ThermoFisher Scientific (Waltham, MA).

2.2.2 Cell culture media composition

Expansion media (EM) for cell culture contained advanced DMEM/F12 medium, L-WRN conditioned medium, HEPES (10 mM, pH 7.5), EGF (50 ng/mL), GlutaMAX (2 mM), priomcin (100 µg/mL), and Y-27632 ROCK inhibitor (10 µM). As previously outlined by Stappenbeck et al., L-WRN conditioned medium was prepared by the culturing of L-WRN cells (ATCC, #3276) and harvesting Wnt-3A, R-spondin 3, and noggin secreted into the supernatant by cells[38]. Wnt-3A, R-spondin 3, and noggin were used at final concentrations in the culture medium of 30, 75 and 71 ng/mL, respectively. Differentiation media (DM) contained DMEM/F12 medium, HEPES (10mM, pH 7.5), GlutMAX (2 mM), primocin (100 µg/mL), N-acetylcysteine (1.23 mM), EGF (50 ng/mL), and A83-01 (500 nmol/mL).

2.2.3 Primary mouse colon monolayer cell culture

Murine large intestines were collected from both female and male mice between the ages of 6 and 10 weeks. The colonic crypts were isolated using a previously published protocol from the Allbritton group[36]. In summary, the intestinal tissue was cut longitudinally to expose the luminal and basal sides of tissue before being placed in ethylenediaminetetraacetic acid (EDTA, 2 mM) and dithiothretol (DTT, 0.5 mM) in buffer (5.6 mM Na2HPO4, etc.) for 90 minutes at room temperature. Through vigorous shaking the crypts/villi were dissociated and collected by centrifugation. Crypt density was measured using a 10 μL suspension on a petri dish and approximately 1000 crypts/cm^2 distributed per well in a 6-well plate. For the first 48-hours of culture Y-27632 was added to the medium to minimize apoptotic death. The culture media was changed every 48 hours after that. Once cell coverage reached 80% the wells were subcultured involving a 2-step dissociation method. Culture media was aspirated, the collagen scaffold separated from the well using 1-mL pipette tip and transferred to a 15-mL conical tube containing 1 mL of culture media and 500 U/mL of collagenase type IV. A 5-mL and then 1-mL pipette tip were used to mechanically breakdown the collagen further. The conical tube with cells was then incubated at 37°C for 10 minutes. After centrifugation at 600 x g for 1 minute, the cells were washed in 5 mL of 1x PBS. The cells were then further detached from their substrate by incubation in 150 μL EDTA (500 μmol/L), and Y-27632 (10 μmol/L), incubated at 37°C for 2 minutes. This was followed by pipetting 20 to 50 times with a 200 μL pipet tip to disperse the cells. The cells were resuspended in culture media and passaged a ratio of 1:3 onto fresh collagen scaffolds.

2.2.4 Preparation neutralized collagen scaffold

A collagen hydrogel was prepared using a custom neutralization buffer to neutralize the acidic collagen solution to a final pH of 7.4 as previously described[36]. The neutralization buffer (consisting of HEPES, NaHCO3, NaOH in 10x PBS, and deionized water) was sterile filtered prior to use and stored at room temperature for up to 1 month before use. The neutralization buffer was placed in 4°C for 15 minutes before mixing it with a collagen stock solution to reach a final concentration of 1mg/mL collage protein. The mixture (1mL) was added to each well of a 6-well plate and incubated for 1 hour at 37°C to produce a clear hydrogel. After incubation, 2 mL of PBS was added to each well and stored in the incubator at 37°C until use.

2.2.5 Microscopy Setup

An inverted TE300 Nikon microscope (Nikon Instruments Inc., Melville, NY) equipped with a CoolSNAP Myo CCD camera (Photometrics, Tucson, AZ) was used for all experimental imaging. The microscope was fit with a PS3H122R motorized focus drive and H138A motorized XY translational stage fit to the microscope with a custom-made adapter and controlled through a ProScan III Controller (Prior Scientific Inc., Rockland, MA). The two objectives utilized during experimentation were a Plan Fluor 4x, and an ELWD Plan Fluor 40x objective (0.60 and 0.13 NA respectively, Nikon Instruments Inc., Melville, NY). A filter set containing a UV-2E/C and B-2E/C filter cubes (excitation: 360 ± 20nm and 480 ± 15 nm, emission: 460 ± 25 nm and 535 ± 20 nm, Nikon Instruments Inc., Melville, NY) permitted imaging in the blue and green wavelengths. One filter slot was left empty for full pass through and brightfield imaging. Excitation light was provided by a Lumen 200 arc lamp (Prior Scientific Inc., Rockland, MA). A *Smart*Shutter (IQ12-SA) in combination with a Lamba-SC (Sutter Instrument, Novato, CA) was used to control exposure. The focus drive, microscope stage, camera, and shutter were controlled

by custom software written in MATLAB (MathWorks, Natick, MA) and using a Micro-Manager (Open Imaging, San Francisco, CA) core[39, 40]. A custom-made enclosure was built from polycarbonate panels to maintain an imaging temperature of 37°C and a humidity of >45% during imaging, regulated by an Air-Therm SMT (World Precision Instruments, Sarasota, FL).

2.2.6 Fluorescent imaging of intracellular Ca2+

Culture plates were placed in the tissue culture hood and culture media replaced with a calcium-indicator loading media, which consisted of the base media the cells were already in (i.e. expansion media or differentiation media) with 1% Pluronic-F127 and 2% Probenecid. Either Cal-520 AM or Fluo-4 AM at a concentration of 5 μM was added to the wells and returned to the incubator for 30 minutes. For the final 30 minute of loading, Hoechst 33342 was included for cell viability. After incubation the cell plate was moved to a tissue culture hood, rinsed three times with 1x PBS and then resupplied with fresh loading media. The plate was transferred to a custom microscope stage insert within a custom incubation chamber remain at 37°C and >40% humidity. The well for imaging was selected and a brightfield area scan performed using the 4x objective, with a 5% overlap between fields of view and automated focus algorithm as previously described[41]. The images were then stitched, and high magnification imaging sites selected based on present cell patches (Figure 2.3). Brightfield imaging and Hoechst 33342 fluorescent imaging was performed at each site using the 40x objective. Calcium fluorescent images using either Cal-520 or Fluo-4 were then collected for each site at 2 second time points (Gain 1, Binning 2) for a total of 12 minutes resulting in a temporal image stack of 360 images.

2.2.7 Statistical Analysis

Graphpad Prism 8.3 was used for all statistical analysis (GraphPad Software, Inc. La Jolla, CA). Multi comparisons were performed using a one-way ANOVA and Tukey's test. All

statistical tests were performed at the 5% significance levels. Measurements are reported as the ± the standard deviation unless otherwise noted. For all statistical comparisons, p values are represented following the American Psychological Association (APA) style[42] of * for $p< 0.05$, ** for $p<0.01$, and *** for $p<0.001$.

2.3 Results and Discussion

2.3.1 Identification of calcium signaling in primary colon monolayer

Fluorescent Ca^{2+} imaging was performed on expanding patches of primary mouse colon cells as a preliminary investigation to determine the presence of Ca^{2+} signaling. The 2D colon culture protocol developed by Wang et al., provides patches of multiple cell types with differentiated cells in the center and actively proliferating cells at the edges[36]. Self-renewing monolayer of primary mouse colon cells on collagen scaffolding (1mg/mL) were prepared and cells were kept in expansion media, changed every two days. Individual wells were imaged at 24-hour time points post cell seeding to capture different cell populations as the cells expanded into a confluent monolayer, usually occurring around day 4 post passage. Imaging began with an automated area scan and image stitch using the 4x objective to image the entire well, this allowed for the collection of cell patch morphology and the selection of calcium image sites at a higher magnification (Figure 2.2). With image sites selected, the objective was changed to a 40x long working distance objective for further imaging. Each image site was imaged in bright-field and a Hoechst fluorescent image collected for cell counting and cell viability. Calcium imaging was performed for 12 minutes, capturing images at two second intervals. Calcium imaging was attempted with both Cal-520 AM, and Fluo-4 AM, both selected for their dissociation coefficients (320 and 345 nM) (Table 2.3). Based on the larger quantum yield and a smaller

degree of compartmentalization at 37 °C, Cal-520 AM was selected for all future calcium imaging (Figure 2.2).

To identify the presence of calcium signaling the raw image stacks were first manually inspected. If calcium signals were found to be present a best fit ROI was drawn. The mean fluorescence for these ROIs was measured across time and a signal profile constructed. Using the standard limit of detection (LOD) and previously utilized thresholds for neuronal calcium traces as reference, Ca^{2+} peak detection was thresholded at three times the standard deviation of the signal[22, 23, 43]. A minimum spacing of six seconds (three frames) was also implemented, accounting for Nyquist sampling and preventing multiple identifications of a single peak[44]. A final percentage of cells with Ca^{2+} oscillations present was calculated using a total cell count from Hoechst fluorescence images for each image site. The mean percentage of signaling cells showed a significant difference ($p<0.001$) between different timepoints following passaging (Figure 2.5, n = 6 image sites for each time point). Inspecting the results, largest mean percentage of signaling cells occurred within 48 hours following passaging, with a mean of 11.9 ± 7.2% and 10.3 ± 3.9% of signaling cells at 24 hours and 48 hours. There was a significant decrease ($p<0.05$) in the mean percentage of signaling cells with 5.8 ± 1.9% at 72 hours, 4.0 ± 1.3% at 96 hours, 1.9 ± 0.4% at 120 hours, and 2.0 ± 0.8% at the final timepoint 144 hours. These results demonstrate the feasibility of Ca^{2+} imaging on the 2D primary mouse colon culture and a robust collection of Ca^{2+} signals present.

2.3.2 Ca2+ image analysis and optimization

After confirming the presence of Ca^{2+} oscillation within primary colonic epithelium, the following investigations were aimed towards constructing an image analysis pipeline for the isolation of the Ca^{2+} signals. Desirable attributes for the pipeline included the capability of

automation, accurate cell identification, and removal of background fluorescence. The main challenges the pipeline faced were neighboring cell signals, fluctuating fluorescent background, and Ca^{2+} indicator photobleaching. These are not uncommon problems in fluorescent imaging and reviewing previous literature yielded a vast range of Ca^{2+} image analysis tools[20–23, 45]. Reviewing these methods, a final collection was collated for potential implementation based on their availability, range of customization, compatibility with MATLAB and provided support documentation (Table 2.1). Signal isolation was then attempted on the previously collected Ca^{2+} image sets with each package and their function assessed. Based on the implantation of each, the CaImAn/CNMF-E packaged proved the most versatile in isolating signals and removing both the global and local background (Fig. 2.3).

With a toolkit selected for signal isolation, a basic pipeline was implemented using MATLAB and the public GitHub repositories for the MATLAB packages of CNMF-E and CaImAn[23]. To assess and optimize the pipeline's initial performance in accurately segmenting cells undergoing calcium oscillations, a comparison set was manually constructed from the previously collected calcium image data. Areas of calcium activity were identified in the temporal image stack and manually outlined. These outlines were then transposed onto the Hoechst fluorescence image of the same image site and used to link the area of calcium activity to a specific nucleus. These nuclei were manually outlined, and the associated pixels were used as positive control pixels during optimization (Figure 2.7). The CaImAn toolbox was designed to be automated with limited user input with the exception of certain variables used to modify the toolbox for different experimental data[22]. The first of these variables is the kernel used in the initial Gaussian spatial filtering and depends on the mean diameter of the cells image (Figure 2.6). The applied filtering reduces background noise while enhancing any objects with a smaller

diameter than the Gaussian kernel which in this application are the oscillating cells. The next variables are minimum local correlation and minimum peak-to-noise ratio (PNR) of seeding pixels (Figure 2.6). These seed pixels create regions of interest (ROIs) within the image stack for greedy initialization, which defines the starting cellular spatial components (C) in the base model for constrained non-negative matrix factorization (CNMF) shown below.

$$(2.1) \quad Y = AC + B + E$$

Where Y is the three-dimensional matrix of pixels values, C is the spatial footprint of target cells, A is the calcium activity of targets cells, B is the fluctuating background and E is uncorrelated noise. The pipeline is then run fully automated, iteratively fitting the model until final components are found to fit the constrained non-negative matrix. In processing the final components, there exist multiple possible automated and manual interventions. For the purposes of the optimization no manual interventions were introduced. The value range for the Gaussian kernel was based on previously murine colon crypt cell measurements and set between 10 and 60 pixels (2 to 9 μm cell diameter)[46]. The tested value ranges for the minimum local correlation and PNR were based on previous work with the CaImAn toolbox, set between 0.5 to 0.9 and 3 to 15, respectively. The performance of each parameter value combination was then assessed using F-score statistical analysis, commonly used for calculating the accuracy of binary classifier[47] (Eq. 2.2). The F-score includes assessing the ability in minimizing false positives (precision) and ability to identify all true positives (recall).

$$(2.2) \; F\ Score = 2 \times \frac{Precession \times Recall}{Precission + Recall}$$

For the purposes of this performance evaluation, recall was quantified based on the identification true pixels outlined in the test data (Eq. 2.3, Figure 2.7). Due to the limitations of determining clear cell borders in the colon epithelium patches, precision was quantified based on the ability accurately identify the total number of cells with Ca^{2+} oscillations (Eq. 2.4).

$$(2.3)\ Recall = \frac{True\ Positive\ Pixels}{True\ Positive\ Pixels + False\ Negative\ Pixels}$$

$$(2.4)\ Precision = \frac{True\ Postive\ Cells}{Manual\ Cell\ Count + False\ Postive\ Cells}$$

The different combinations of parameters were tested on 7 separate manual test sets and the F-score calculated. Optimal performance was found using a PNR threshold of 5, local correlation of 0.8, and a Gaussian kernel of 13 pixels (~2 μm) which resulted in a mean F-score of 0.74 ± 0.14 (Scale of 1 to 0, with 1 being a perfect pixel classification, Figure 2.7). The associated average runtime was 159 ± 36 seconds.

2.3.3 Spatio-temporal characteristics under basic culture conditions

The newly optimized image pipeline was used to collect cell Ca^{2+} signals from the original image stacks and characterize their spatial-temporal properties. Similar spike thresholds and signal deconvolution from the neuron action potential imaging were employed and allowed high throughput of signal analysis[20, 37]. To allow for increased throughput different curve fitting approaches were investigated to automate the pulse width measurements of isolated oscillations. The attempted approaches included Gaussian, Lorentzian and flat top fitting strategies as outlined by O'Haver, T, with linear, quadratic, and flat background correction included[48, 49]. Custom MATLAB scripts were written and also included using the functions *findpeaks* and *pulsewidth* from the MATLAB processing toolkit. To assess the pulse width measurement

accuracy of each method, sample cell signals with varying pulse widths were selected and a total of 25 peaks manually measured (Fig 2.8). The different curve fitting methods were then applied to each signal and resulted in the *findpeaks* script showing the least mean error in pulse width measurement (Figure 2.8, 6.5 ± 4.2 seconds mean error). To quantify the total peaks and the mean pulse width, isolated signals with background subtraction were processed using a custom MATLAB script. The *findPeaks* command from MATLAB signal processing toolkit was performed on each signal profile, using a threshold of three times the standard deviation calculated from the original signal and within a search window of 10 seconds. The resulting signals and their identified peaks were then manually inspected to filter any misidentified peaks. The sum of peaks was calculated for each signal and their pulse width calculated using the output from the find peaks command. The highest mean peak count was 24 hours post passage at 6.3 ± 4.2 peaks over 12 minutes, and significantly higher than the following five days 4.3 ± 3.8, 3.4 ± 2.6, 2.5 ± 2.2, 2.1 ± 1.2, and 1.9 ± 2.0 peaks over 12 minutes respectively (Figure 2.9, 24 hrs: 5 signals, 48 hrs: 7 signals, 72 hrs: 6 signals, 96 hrs: 7 signals, 120 hrs: 6 signals, 144 hrs: 6 signals). The mean pulse widths within the first three time points post passage were 20.3 ± 5.6, 20.2 ± 6.5, and 34.3 ± 19.6 seconds respectively and 35.7 ± 23.0, 37.8 ± 21.5, and 45.1 ± 24.4 seconds for the following three timepoints. There is a substantial increase in standard deviation in collection pulse widths over the six days post passage, from 5.6 to 24.4 seconds, suggesting an increase signal heterogeneity in parallel with the colon cells as they expand to confluency. When compared with similar signals found in the *Drosophila* model, the measurements vary most in pulse width which is not unexpected consider the mass difference between the mouse model[50].

2.4 Conclusions

Ca^{2+} remains a vital secondary messenger especially in the intestinal epithelium yet limited investigation has been done on its presence and signaling characterization in a primary mammalian model. The 2D self-renewing colon monolayer culture method developed by the Allbritton group provides a platform to study calcium signaling within primary colon crypts using non-genetic calcium indicators. Performing calcium imaging on these monolayers using Cal-520 AM demonstrated the presence of diverse signaling occurring within the epithelium. To isolate these signals an image analysis pipeline based on the CaImAn toolbox, originally designed for neuron signaling, was constructed and optimized for the murine colon cell patches.

2.5 Figures

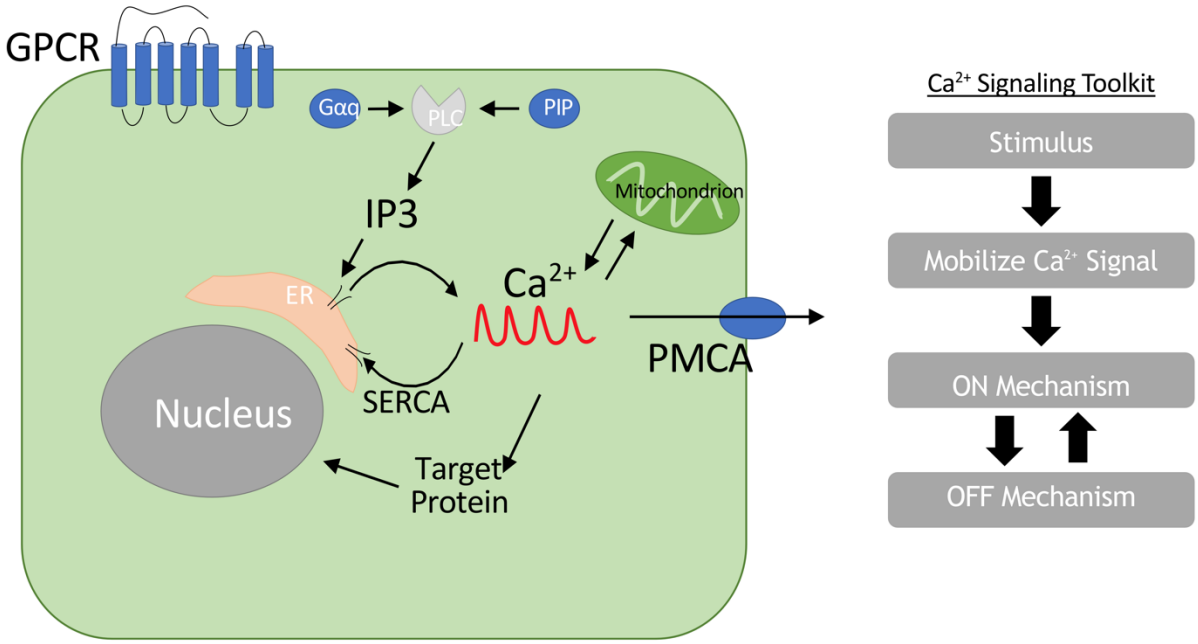

Figure 2.1 Basic sample signaling pathway utilizing Ca^{2+} oscillations (left), showing the core components necessary for Ca^{2+} oscillations (right). When G protein-coupled receptor (GPCR) binds to an extracellular substance (stimulus) it activates phospholipase C (PLC). PLC then hydrolyzes phosphatidylinositol 4,5-bisphosphate (PIP2) to generate secondary messengers 1,4,5-triphosphate (IP3) and diacylglycerol (DAG). IP3 binds with IP3 receptors (IP3R) on the endoplasmic reticulum (ER) releasing the cell's stored Ca^{2+} into the cytosol (ON mechanism). The cytosolic Ca^{2+} can then be decrease multiple ways including reuptake into the ER by sarcoendoplasmic reticulum calcium transport ATPase (SERCA), uptake and release by the mitochondria, or removal from the cell through plasma membrane Ca^{2+} ATPase (PMCA, OFF mechanism). The resulting Ca^{2+} oscillations can activate downstream targets such as calcineurin (CaN) which goes on to activate the transcription factor NFAT.

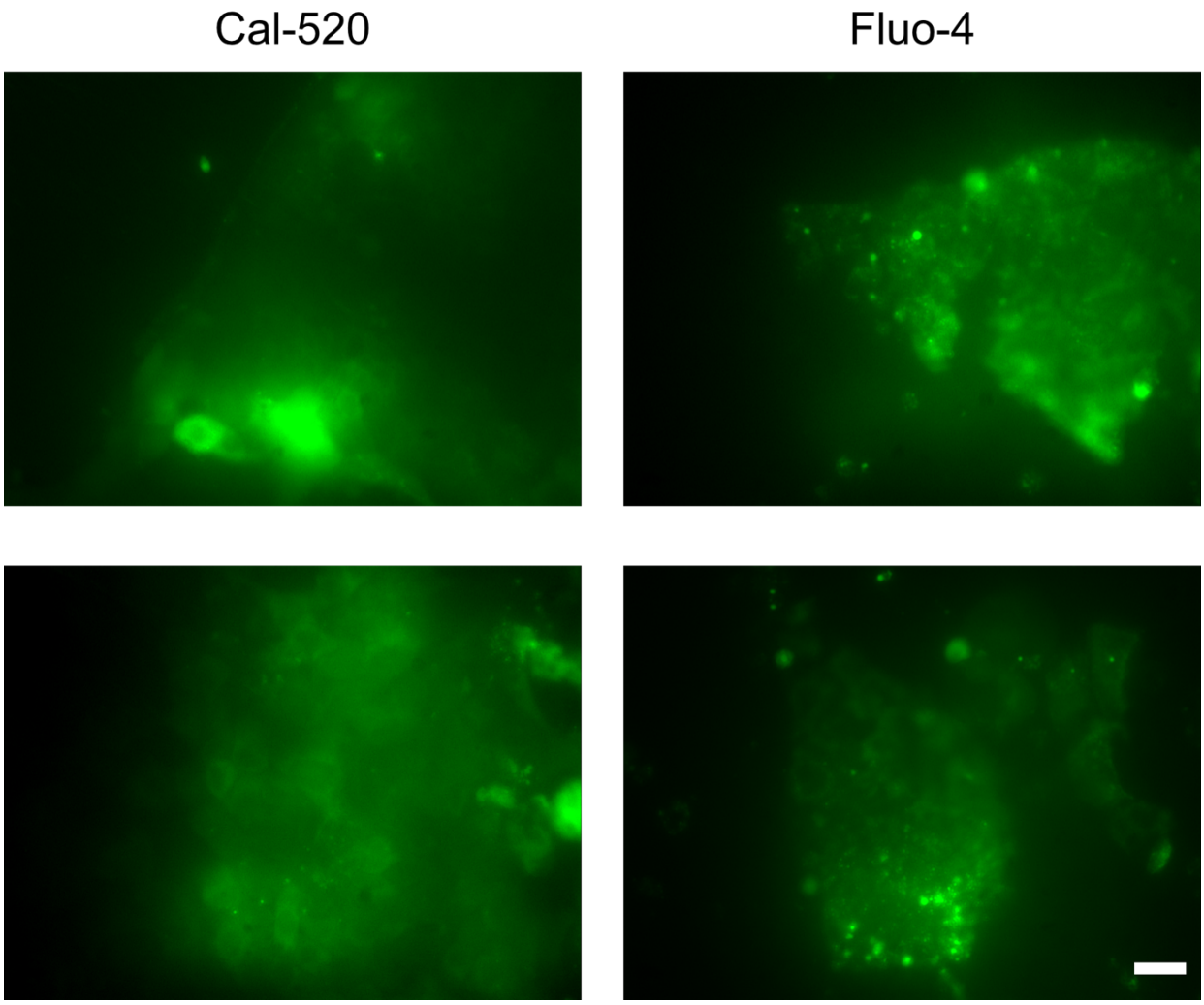

Figure 2.2 Comparison between Ca^{2+} indicators Cal-520 AM and Fluo-4 AM. For each indicator, loading was performed at a concentration of 5 µM for 1 hour at 37 °C. Images were collected at 37 °C immediately after loading and washing three times with 1 x PBS. Scale bar = 25 µm

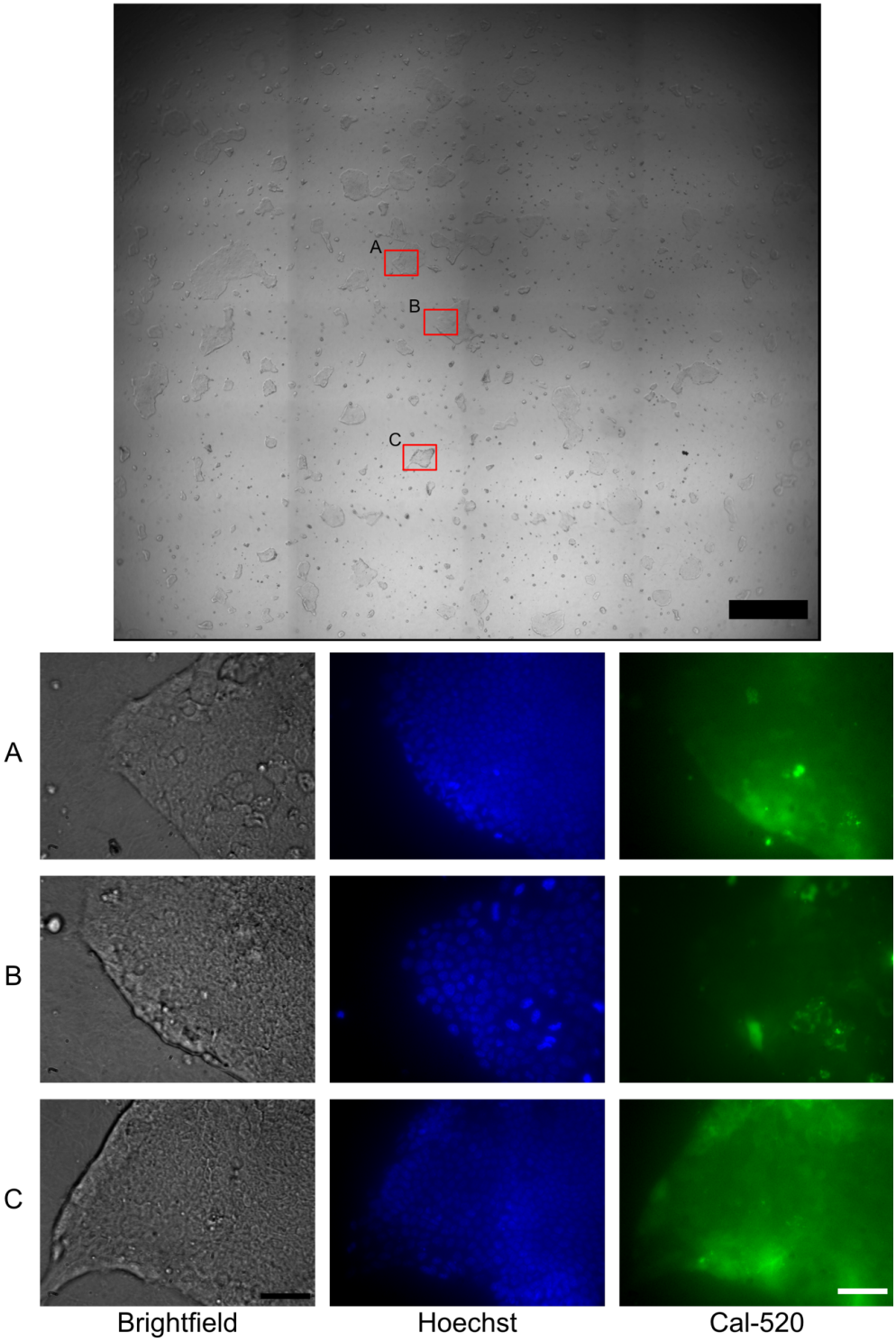

Figure 2.3 Example of area scan performed with 4x objective (NA 0.60) with post image stitching for identification of possible image sites (Scale bar = 250 µm). Below, three sample image sites identified in the area scan and imaged with 40x objective at 37 °C (NA 0.13, scale bar = 50 µm)

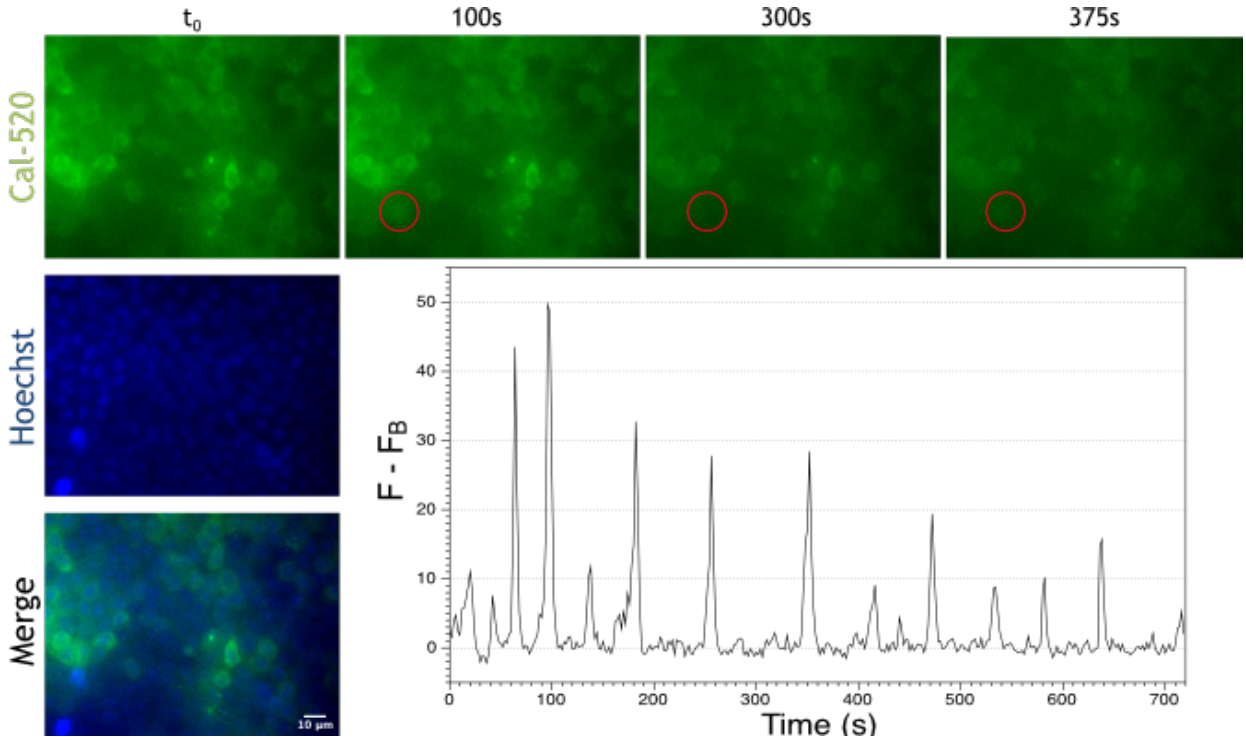

Figure 2.4 A sample cell signal with background fluorescence subtracted. A total of 360 images were captured at 2 second timepoints.

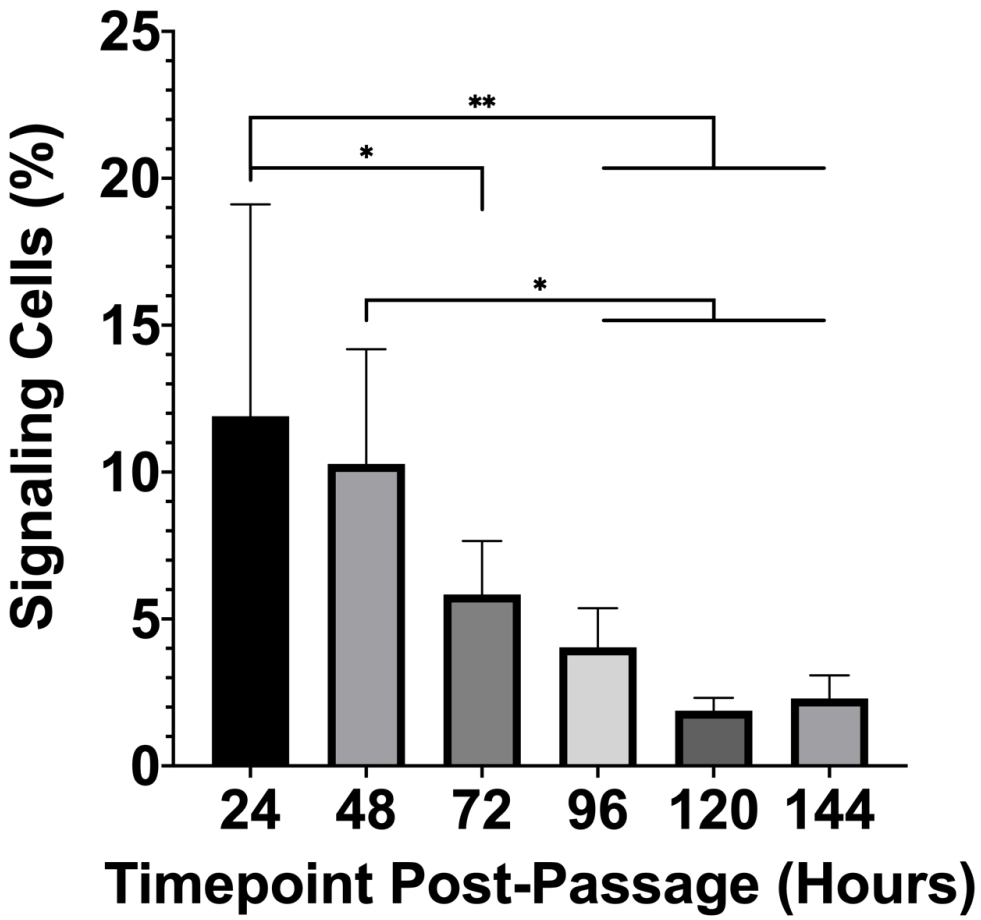

Figure 2.5 The average percentage of cells demonstrating Ca^{2+} fluctuations at different time points post passage. Values represent the mean across 6 images sites for each time point post passage, with the total number of cells quantified from associated Hoechst fluorescent image. Whiskers represent standard deviation. Colon cells were cultured in EM, with media changes at 48 and 92 hours post passage.

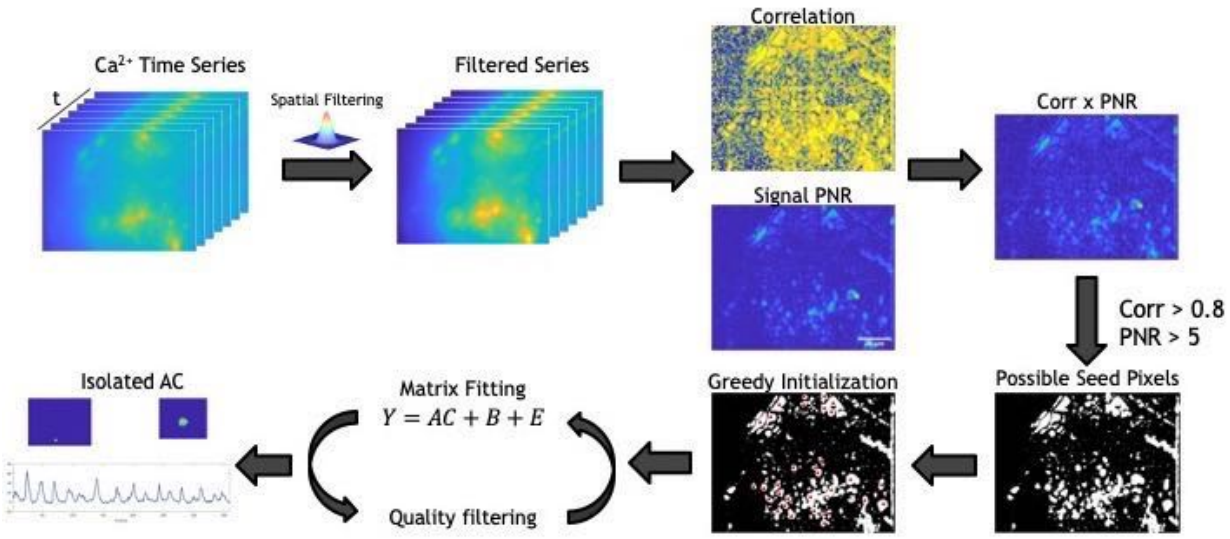

Figure 2.6 A simplified flow diagram of the image analysis pipeline utilizing the CaImAn and CNMF-E packages. The pipeline begins with the capture of a Ca^{2+} time series using the Cal-520 Ca^{2+} indicator. The temporal image stack is then spatial filtered across the entire stack using Gaussian kernel (13) to remove background noise. Using the CaImAn package, a local correlation and signal PNR image are constructed from the temporal image stack. Using different thresholds for local correlation and PNR, areas are identified for suitable signal extraction (seed points) and used to initialize the matrix factorization. For this analysis pipeline the *GreedyCorr* initialization is used for the initial fitting of the CNMF model. The matrix is then iteratively fit to the CNMF model until the components reach a stabilized residual sum of squares (RSS), normally 3 to 5 cycles. The final outputs are the isolated fluorescent profiles (A) and the associated cell areas (C).

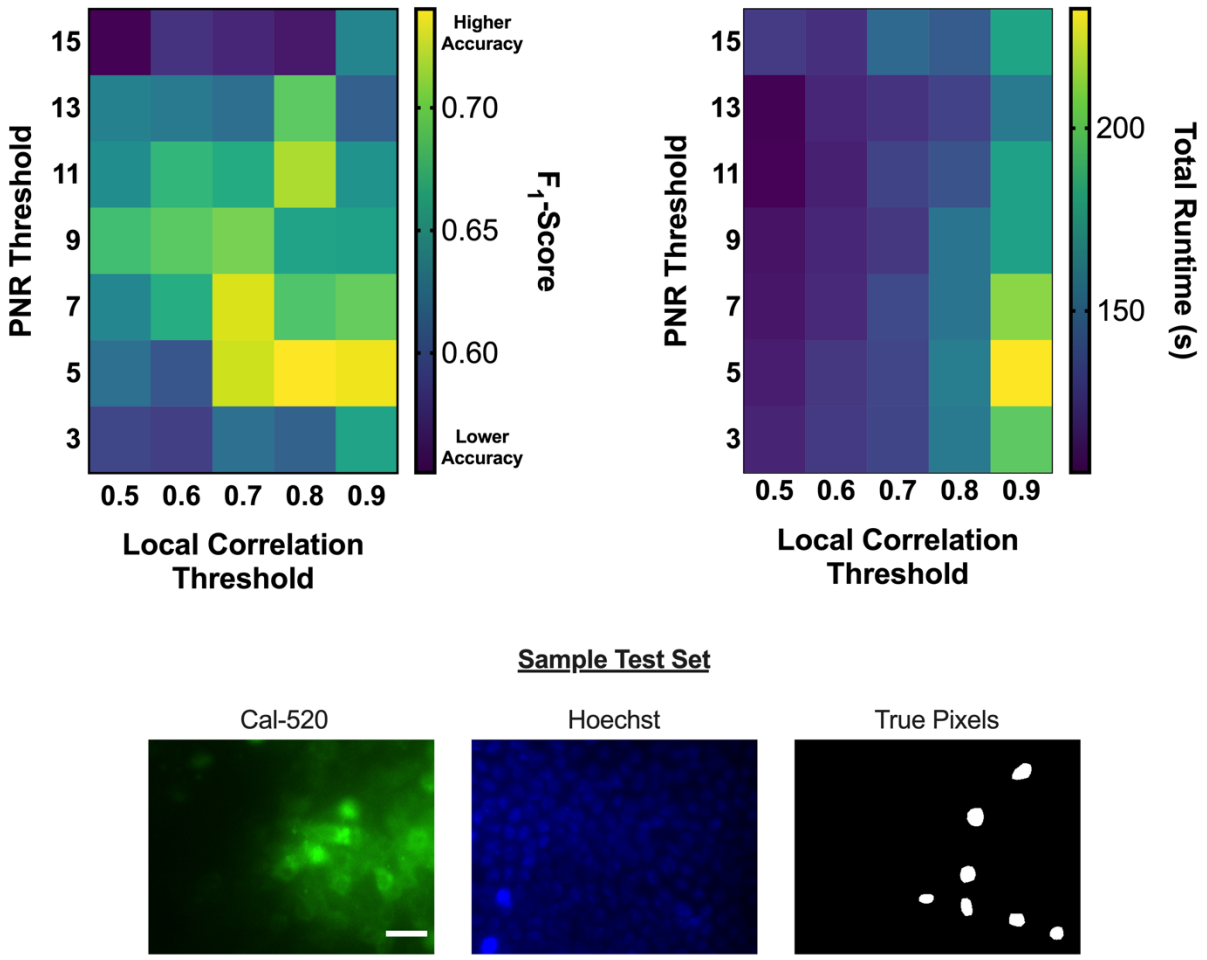

Figure 2.7 A heat map showing the mean F-Score (top left) of the image analysis pipeline given a certain PNR and local correlation threshold for the initialization of the constrained non-negative matrix factorization (CNMF, a total of 7 test sets were used). The F-score ranges from 1 to 0, with 1 being a perfect identification of true positives. The mean total runtime for a single image site is also shown (top right) given a certain PNR and local correlation threshold. A sample test constructed for image analysis pipeline optimization, including fluorescent image of Cal-520 at t = 0 and true pixels defined by outlining nuclei of cells exhibiting Ca^{2+} fluctuations (Scale bar = 10 μm).

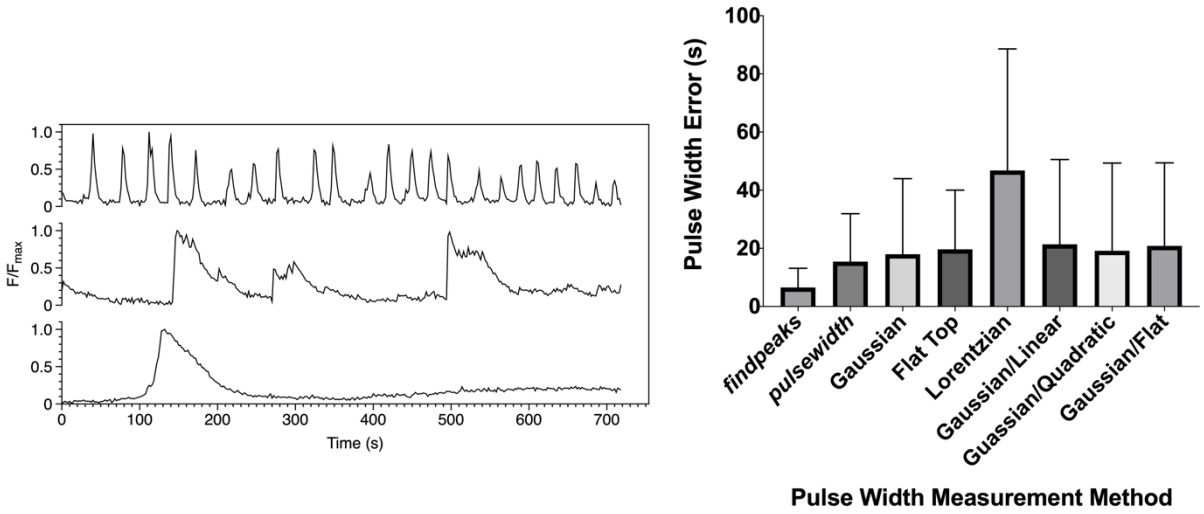

Figure 2.8 Sample cell signals (left) used to test different methods for automated pulse width measurement. The modeled CNMF background has been subtracted and each signal has been normalized to its maximum fluorescence. The mean pulse width error (right) of different methods for pulse modeling (n = 3 cell signals, 25 pulses). Whiskers represent standard deviation.

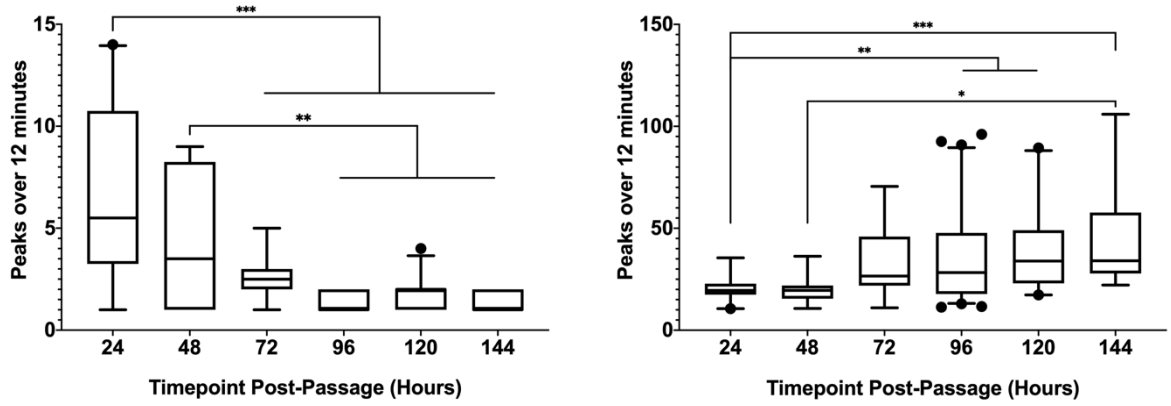

Figure 2.9 Box-and-whisker plots showing distributions of total Ca^{2+} oscillations and mean pulse widths of Ca^{2+} signals at different timepoints following passaging on neutralized collagen. Boxes are centered on the median and extends to the 25^{th} and 75^{th} percentiles, while the whiskers extend to the 5^{th} and 95^{th} percentiles. The number of cells included for each time point were 5 cells for 24 hrs, 7 cells for 48 hrs, 6 cells for 72 hrs, 7 cells for 96 hrs, 6 cells for 120 hrs, and 6 cells for 144 hrs.

2.6 Tables

Table 2.1 List of different neuron image analysis packages, all packages offer motion correction, signal isolation and deconvolution

Method Name	Original Application	Platforms
CaImAn[22]	1-photon, 2-photon	Matlab, Python
CaImAn CNMF-E[23]	1-photon endoscope	Matlab
NeuroCa[20]	1-photon	Matlab
Min1Pipe[21]	1-photon endoscope	Matlab, Python
Suite2p[19]	2-photon	Python
AQuA[51]	2-photon	Matlab, Python

Table 2.2 Comparison between Ca^{2+} indicators

Ca^{2+} Indicator	Dissociation Coefficient	Quantum Yield	Excitation Wavelength (nm)	Emission Wavelength (nm)
Fluo-4 AM[52, 53]	345	0.15	494	516
Cal-520 AM[16]	320	0.75	492	514

REFERENCES

1. La Rovere RML, Roest G, Bultynck G, Parys JB. Intracellular Ca 2+ signaling and Ca 2+ microdomains in the control of cell survival, apoptosis and autophagy. Cell Calcium. 2016;60:74-87.

2. McLaughlin S, Smith SO, Hayman MJ, Murray D. An electrostatic engine model for autoinhibition and activation of the epidermal growth factor receptor (EGFR/ErbB) family. J Gen Physiol. 2005;126:41-53.

3. Dolmetsch RE, Lewis RS, Goodnowt CC, Healyt JI. Differential activation of transcription factors induced by Ca2+ response amplitude and duration. Nature. 1997;386124:855-858.

4. Trump BF, Berezesky IK, Sato T. Cell calcium, cell injury and cell death. Environmental Health Perspectives. 1984;VOL. 57:281-287.

5. Bers DM. Cardiac excitation-contraction coupling. Nature. 2002;415:101-132.

6. Dupont G, Combettes L, Bird GS, Putney JW. Calcium oscillations. Cold Spring Harb Perspect Biol. 2011;3

7. Noren DP, Chou WH, Lee SH et al. Endothelial cells decode VEGF-mediated Ca2+ signaling patterns to produce distinct functional responses. Sci Signal. 2016;9:ra20.

8. Leiper LJ, Walczysko P, Kucerova R et al. The roles of calcium signaling and ERK1/2 phosphorylation in a Pax6+/- mouse model of epithelial wound-healing delay. BMC Biol. 2006;4:27.

9. Aihara E, Hentz CL, Korman AM et al. In vivo epithelial wound repair requires mobilization of endogenous intracellular and extracellular calcium. J Biol Chem. 2013;288:33585-33597.

10. Minta A, Kao JPY, Tsien RY. Fluorescent indicators for cytosolic calcium based on rhodamine and fluorescein chromophores. Journal of Biological Chemistry. 1989;264:8171-8178.

11. Grynkiewicz G, Poenie M, Tsien RY. A new generation of Ca2+ indicators with greatly improved fluorescence properties. Journal of Biological Chemistry. 1985;260:3440-3450.

12. Tsien RY. A non-disruptive technique for loading calcium buffers and indicators into cells. Nature. 1981;290:527-528.

13. Hyrc KL, Minta A, Escamilla PR, Chan PP, Meshik XA, Goldberg MP. Synthesis and properties of Asante Calcium Red--a novel family of long excitation wavelength calcium indicators. Cell Calcium. 2013;54:320-333.

14. Tian L, Hires SA, Mao T et al. Imaging neural activity in worms, flies and mice with improved GCaMP calcium indicators. Nature Methods. 2009;6:875-881.

15. Russell JT. Imaging calcium signals in vivo: A powerful tool in physiology and pharmacology. British Journal of Pharmacology. 2011;163:1605-1625.

16. Lock JTDON, Behavior UOC, Irvine, CA, Parker I, Smith IFDON, Behavior UOC, Irvine, CA. A comparison of fluorescent Ca2+ indicators for imaging local Ca2+ signals in cultured cells. Cell Calcium. 2016;34:352-359.

17. Göbel W, Helmchen F. In vivo calcium imaging of neural network function. Physiology (Bethesda). 2007;22:358-365.

18. Stringer C, Pachitariu M. Computational processing of neural recordings from calcium imaging data. Current Opinion in Neurobiology. 2019;55:22-31.

19. Pachitariu M, Stringer C, Dipoppa M et al. Suite2p: beyond 10,000 neurons with standard two-photon microscopy. 2016

20. Jang MJ, Nam Y. NeuroCa: integrated framework for systematic analysis of spatiotemporal neuronal activity patterns from large-scale optical recording data. Neurophotonics. 2015;2:035003.

21. Lu J, Li C, Singh-Alvarado J et al. MIN1PIPE: A Miniscope 1-Photon-Based Calcium Imaging Signal Extraction Pipeline. Cell Rep. 2018;23:3673-3684.

22. Giovannucci A, Friedrich J, Gunn P et al. CaImAn: An open source tool for scalable Calcium Imaging data Analysis. bioRxiv. 2018339564.

23. Zhou P, Resendez SL, Rodriguez-Romaguera J et al. Efficient and accurate extraction of in vivo calcium signals from microendoscopic video data. Elife. 2018;7

24. Brodskiy PA, Zartman JJ. Calcium as a signal integrator in developing epithelial tissues. Physical Biology. 2018;15

25. Crossman MW, Hauft SM, Gordon JI. The mouse ileal lipid-binding protein gene: A model for studying axial patterning during gut morphogenesis. Journal of Cell Biology. 1994;126:1547-1564.

26. Potten CS, Kellett M, Roberts SA, Rew DA, Wilson GD. Measurement of in vivo proliferation in human colorectal mucosa using bromodeoxyuridine. Gut. 1992;33:71-78.

27. Barker N, van Es JH, Kuipers J et al. Identification of stem cells in small intestine and colon by marker gene Lgr5. Nature. 2007;449:1003-1007.

28. Sangiorgi E, Capecchi MR. Bmi1 is expressed in vivo in intestinal stem cells. Nat Genet. 2008;40:915-920.

29. Shah P, Fritz JV, Glaab E et al. A microfluidics-based in vitro model of the gastrointestinal human-microbe interface. Nat Commun. 2016;7:11535.

30. Sung JH, Yu J, Luo D, Shuler ML, March JC. Microscale 3-D hydrogel scaffold for biomimetic gastrointestinal (GI) tract model. Lab Chip. 2011;11:389-392.

31. Sun H, Chow ECY, Liu S, Du Y, Pang KS. The Caco-2 cell monolayer: Usefulness and limitations. Expert Opinion on Drug Metabolism and Toxicology. 2008;4:395-411.

32. Hinman S, Wang Y, Allbritton N. Photopatterned Membranes and Chemical Gradients Enable Scalable Phenotypic Organization of Primary Human Colon Epithelial Models Photopatterned Membranes and Chemical Gradients Enable Scalable Phenotypic Organization of Primary Human Colon Epithelial Mode. 2019

33. Kim R, Wang Y, Hwang SHJ et al. Formation of arrays of planar, murine, intestinal crypts possessing a stem/proliferative cell compartment and differentiated cell zone. Lab on a Chip. 2018;18:2202-2213.

34. Yamazaki D, Hasegawa A, Funato Y et al. Cnnm4 deficiency suppresses Ca^{2+} signaling and promotes cell proliferation in the colon epithelia. Oncogene. 2019;38:3962-3969.

35. George L. Calcium signalling in human colonic epithelium. In press 2019.

36. Wang Y, DiSalvo M, Gunasekara DB et al. Self-renewing Monolayer of Primary Colonic or Rectal Epithelial Cells. Cmgh. 2017;4:165-182.e7.

37. Giovannucci A, Friedrich J, Deverett B, Staneva V, Chklovskii DB, Pnevmatikakis EA. CaImAn-MATLAB version 6bd51e2. GitHub

38. Miyoshi H, Stappenbeck TS. In vitro expansion and genetic modification of gastrointestinal stem cells in spheroid culture. Nat Protoc. 2013;8:2471-2482.

39. Edelstein A, Amodaj N, Hoover K, Vale R, Stuurman N. Computer control of microscopes using μManager. Curr Protoc Mol Biol. 2010;Chapter 14:Unit14.20.

40. Stuurman N, Amdodaj N, Vale R. μManager: Open Source Software for Light Microscope Imaging. Microscopy Today. 2007;15:42-43.

41. DiSalvo M, Harris DM, Kantesaria S et al. Characterization of Tensioned PDMS Membranes for Imaging Cytometry on Microraft Arrays. Anal Chem. 2018;90:4792-4800.

42. American PA, others. Publication manual of the American psychological association Washington. DC: American Psychological Association. 2010

43. Protocols for Determination of Limits of Detection and Limits of Quantitation; Approved Guidelines. 2004; 2004.

44. Nyquist H. Certain Topics in Telegraph Transmission Theory. Transactions of the American Institute of Electrical Engineers. 1928;47:617-644.

45. Ellefsen KL, Settle B, Parker I, Smith IF. An algorithm for automated detection, localization and measurement of local calcium signals from camera-based imaging. Cell Calcium. 2014;56:147-156.

46. Dunn SJ, Appleton PL, Nelson SA, Näthke IS, Gavaghan DJ, Osborne JM. A two-dimensional model of the colonic crypt accounting for the role of the basement membrane and pericryptal fibroblast sheath. PLoS Comput Biol. 2012;8:e1002515.

47. Van Rijsbergen CJ. Information retrieval. 1979

48. O'Haver T. Pragmatic Introduction to Signal Processing. Applications in scientific measurement. 2020

49. O'Haver T. iPeak. 2016

50. Nielsen KS. Animal physiology. Prentice-Hall of India (Private) Limited; 1964

51. Wang Y, DelRosso NV, Vaidyanathan TV et al. Accurate quantification of astrocyte and neurotransmitter fluorescence dynamics for single-cell and population-level physiology. Nature Neuroscience. 2019;22:1936-1944.

52. Gee KR, Brown KA, Chen WN, Bishop-Stewart J, Gray D, Johnson I. Chemical and physiological characterization of fluo-4 Ca(2+)-indicator dyes. Cell Calcium. 2000;27:97-106.

53. Paredes RM, Etzler JC, Watts LT, Zheng W, Lechleiter JD. Chemical calcium indicators. Methods. 2008;46:143-151.

CHAPTER 3: THE EFFECTS OF DIFFERENT SIGNALING PATHWAYS ON INTRACELLULAR CA^{2+} SIGNALING IN MURINE COLON EPITHELIUM

3.1 Introduction

A complex collection of gradients exists within the colon crypt stem cell niche, balancing proliferation and differentiation[1]. Key regulatory signals within the colon crypt include conical Wnt signaling, bone morphogenetic protein (BMP), and Notch signaling pathways. Wnt and Notch signaling is largest at the base of the colon crypt promoting ISC self-renewal[2]. Homeostatic Notch signaling results in progenitor cells predominately differentiating into absorptive cells but when decreased shift to secretory cell fates[3]. At the luminal end of the crypt, are elevated concentrations of BMP-2 and BMP-4 secreted by inter-crypt mesenchymal cells[4]. BMP signaling promotes differentiation through the Smad-mediated transcriptional repression of multiple signature genes that promote stemness[5]. The intestine is also host to microbiota, which produce a vast array of metabolites such as polyamines and short-chain fatty acids (SCFAs)[6–8]. The crypt structure decreases the exposure of these metabolites to ISCs and progenitors. A screen of 92 molecules showed butyrate, a product of the bacterial fermentation of dietary fiber, as a potent suppressor of proliferation even with Wnt signaling present[9]. The extracellular matrix surrounding the colon crypt exhibit gradients, aiding in the promotion of proliferation or differentiation of colon cells. Through the advancement of in vitro culture methods, 1.3 kPa of has been found as an optimal scaffold stiffness for the promotion of colon cell proliferation[10].

Investigating the metabotropic glutamate receptor (mGluR) in Drosophila midguts, Deng et al. demonstrated Ca^{2+} acting as a diverse signal integrator regulating ISC proliferation[11]. The ISCs in freshly resected wild type midguts showed frequent Ca^{2+} oscillations through the use of a genetical encoded Ca^{2+} receptor (USA-GCamP3) and two-photon microscopy. Increased activation of mGluR activated a signaling cascade involving phospholipase C (PLC) and inositol-1,4,5-triphosphate (InsP3), and InsP3 receptor mediated release of Ca^{2+} from the endoplasmic reticulum (ER). The Ca^{2+} oscillations were still present but now at a decreased frequency and larger amplitude, resulting in a cumulative increase of Ca^{2+} within the cytosol. The elevated cytosolic Ca^{2+} lead to the downstream signaling of the serine/threonine phosphatase calcineurin and increase proliferation in ISCs. Inversely, genetic manipulations to this signaling pathway lead to an increased frequency of oscillations and a decrease of cumulative cytosolic Ca^{2+}. The Ras, JNK, JAK/Stat and insulin receptor (InR) signaling pathways were found to increase ISC proliferation also through increased cytosolic Ca^{2+}[12].

A similar association between cytosolic Ca^{2+} and increased ISC proliferation has been shown in primary colon cells. Lines et al. investigation into the cholinergic calcium signaling pathway in primary human colon crypts showed robust calcium waves propagating along the crypt axis and across multiple cell types[13]. Increased activation of muscarinic-induced acetylcholine receptors with the agonist oxotremorine showed increased cytosolic Ca^{2+} from both ER release and intake from the extracellular environment. Primary colonic organoids exposed to 1 μM oxotremorine showed a significant increase in expansion, although the immunohistochemistry data remained unpublished. A similar association has also been shown in primary mouse colon organoids with Ca^{2+} intake through transient receptor potential cation

channel, subfamily V, member 1 (TRPV1), which suppresses epidermal growth factor receptor (EGFR)[14, 15]. The study of Ca^{2+} signaling in primary mammalian colon cells in response to the different gradients within the colon crypts remains limited.

The aim of the present work was to investigate the impact of different gradients present within the colon crypt on the spatial-temporal properties of Ca^{2+} signaling. Using the luminal access made available by the 2D monolayer system, multiple biochemical growth factors were tested. The impact of Wnt and Notch on Ca^{2+} signaling was initially investigated since these proteins are found at higher concentrations at the base of crypt and support ISC self-renewal. The influence of factors supporting differentiation was also investigated using bone morphogenetic proteins (BMPs) and the short-chain fatty acid (SCFA) butyrate, which promote differentiation in cells migrating towards the crypt-lumina juncture. Multiple dietary compounds were also tested, all of which had previously been shown to alter ISC homeostasis (Table 3.1)[16]. Finally, the impact of increased extracellular matrix stiffness on Ca^{2+} signaling was investigated in primary colon cells.

3.2 Materials and Methods

3.2.1 Materials

The following organic Ca^{2+}-dyes in acetoxymethyl (AM) ester form: Fluo-4 (Thermo Fisher Scientific, Waltham, MA) and Cal-520 (Abcam, Cambridge, MA). Dyes were reconstituted with dimethyl sulfoxide (DMSO) to a final concentration of 1 mM and stored, shielded from light, at -20 °C. DMSO, A83-01, and probenecid were obtained from Sigma-Aldirch Corp. (St. Louis, MO). Rat tail type I collagen, 6-well and 24-well polystyrene tissue culture dishes, and HEPES purchased from Corning (Corning, NY). Collagenase (type IV) was

purchased from Worthington Biochemicals (Lakewood, NJ). Murine EGF was obtained from Peprotech (Rock Hill, NJ). Primocin purchased from InvivoGen (San Diego, CA). Y-27632 (A3008-200) purchased from ApexBio Technology (Houston, TX). L-WRN CRL-3276 cell line was purchased from ATCC (Manassas, VA). All other reagents purchased from ThermoFisher Scientific (Waltham, MA).

3.2.2 Preparation of neutralized collagen scaffold

A collagen hydrogel was prepared using a custom neutralization buffer to neutralize the acidic collagen solution to a final pH of 7.4 as previously described[16]. The neutralization buffer (consisting of HEPES, NaHCO3, NaOH in 10x PBS, and deionized water) was sterile filtered prior to use and stored at room temperature for up to 1 month before use. The neutralization buffer was placed in 4°C for 15 minutes before mixing it with a collagen stock solution to reach a final concentration of 1mg/mL collage protein. The mixture (1mL) was added to each well of a 6-well plate and incubated for 1 hour at 37°C to produce a clear hydrogel. After incubation, 2 mL of PBS was added to each well and stored in the incubator at 37°C until use.

3.2.3 Preparation of cross-linked scaffolding

A standard neutralized collagen scaffolding was prepared as previously described, incubating for 1 hour at 37 °C[16]. The culture plate was then removed and each well rinsed with deionized water three times with 5 minutes between each wash. Cross-linking was performed with 60 mM 1-ethyl-3-(dimethylaminopropyl)carbodiimide hydrochloride (EDC) and 15 mM N-hydroxysuccinimide (NHS) in 100 mM 2-(N-morpholino)ethanesulfoni acid (MES) buffer at pH 5.0. Cross-linking reagents were mixed just before adding 1 mL to each well and incubating at 25 °C for one hour. Thereafter the cross-linking mixture was removed, and the entire plate submersed in DI water overnight. The next day plate was removed from the DI water and air

dried on a paper towel. Thereafter, 1 mL of 75% ethanol was added to each well and moved into a tissue culture hood for five minutes after sterilizing the outside of the culture plate. Ethanol was then aspirated and replaced with 1mL 1x PBS and left in the tissue culture with the lid off for 30 minutes, then washed with 1x PBS three times. A thin layer of collagen was formed over the cross-linked scaffold for improved cell adhesion. A solution of 10 µg/mL rat tail collagen was prepared in col PBS and added to each scaffold and incubated either at 37 °C for four hours or overnight at 25 °C. The following day scaffolds were rinsed with 1x PBS and used for colon culture.

3.2.4 Cell culture media composition

Expansion media (EM) for cell culture contained advanced DMEM/F12 medium, L-WRN conditioned medium, HEPES (10 mM, pH 7.5), EGF (50 ng/mL), GlutaMAX (2 mM), priomcin (100 µg/mL), and Y-27632 ROCK inhibitor (10 µM). As previously outlined by Stappenbeck et al., L-WRN conditioned medium was prepared by the culturing of L-WRN cells (ATCC, #3276) and harvesting Wnt-3A, R-spondin 3, and noggin secreted into the supernatant by cells[17]. Wnt-3A, R-spondin 3, and noggin were used at final concentrations in the culture medium of 30, 75 and 71 ng/mL, respectively. Differentiation media (DM) contained DMEM/F12 medium, HEPES (10mM, pH 7.5), GlutMAX (2 mM), primocin (100 µg/mL), N-acetylcysteine (1.23 mM), EGF (50 ng/mL), and A83-01 (500 nmol/mL).

3.2.5 Primary mouse colon culture

Murine large intestines were collected from both female and male mice between the ages of 6 and 10 weeks. The colonic crypts were isolated using a previously published protocol from the Allbritton group[16]. In summary, the intestinal tissue was cut longitudinally to expose the luminal and basal sides of tissue before being placed in ethylenediaminetetraacetic acid (EDTA, 2 mM)

and dithiothretol (DTT, 0.5 mM) in buffer (5.6 mM Na2HPO4, etc.) for 90 minutes at room temperature. Through vigorous shaking the crypts/villi were dissociated and collected by centrifugation. Crypt density was measured using a 10 µL suspension on a petri dish and approximately 1000 crypts/cm^2 distributed per well in a 6-well plate. For the first 48-hours of culture Y-27632 was added to the medium to minimize apoptotic death. The culture media was changed every 48 hours after that. Once cell coverage reached 80% the wells were subcultured involving a 2-step dissociation method. Culture media was aspirated, the collagen scaffold separated from the well using 1-mL pipette tip and transferred to a 15-mL conical tube containing 1 mL of culture media and 500 U/mL of collagenase type IV. A 5-mL and then 1-mL pipette tip were used to mechanically breakdown the collagen further. The conical tube with cells was then incubated at 37°C for 10 minutes. After centrifugation at 600 x g for 1 minute, the cells were washed in 5 mL of 1x PBS. The cells were then further detached from their substrate by incubation in 150 µL EDTA (500 µmol/L), and Y-27632 (10 µmol/L), incubated at 37°C for 2 minutes. This was followed by pipetting 20 to 50 times with a 200 µL pipet tip to disperse the cells. The cells were resuspended in culture media and passaged a ratio of 1:3 onto fresh collagen scaffolds.

3.2.6 Calcium imaging

Culture plates were placed in the tissue culture hood and culture media replaced with a calcium-indicator loading media, which consisted of the base media the cells were already in (*i.e.* expansion media or differentiation media) with 1% Pluronic-F127 and 2% Probenecid. Cal-520 AM was added to the media, at a concentration of 5 µM and the cells were returned to the incubator for a total of one hour. For the final 30 minutes of loading, Hoechst 33342 (0.16 µM) was included for cell counting. After incubation the cell plate was moved to a tissue culture

hood, rinsed three times with 1x PBS and then supplied with fresh loading media. The plate was transferred to a custom insert on the microscope stage within a customized incubation chamber. During imaging the cells remain at 37°C and the surrounding atmosphere was at >40% humidity. A brightfield area scan of the cells was performed using the 4x objective (NA 0.6), with a 5% overlap between fields of view. An automated focus algorithm maintained the appropriate focal plane during imaging as previously described[18]. The images were then stitched together, and higher magnification imaging sites selected based on cells identified over the collagen-covered holes. Brightfield imaging and Hoechst 33342 fluorescent imaging was performed at each site using the 40x objective (NA 0.13). Fluorescent images of the calcium indicator were collected for each site at 2 second time points (Gain 1, Binning 2) for a total of 12 minutes resulting in a temporal image stack of 360 images.

3.2.7 Image analysis and calcium signal isolation

The collected calcium image stacks were first manually inspected to confirm image integrity and the presence of time-varying fluorescence or calcium signals. If fluorescence changes were identified in the image stack, the images were then fed into a cell isolation pipeline written in MATLAB utilizing the Calcium Image Analysis (CaImAn) and constrained non-negative factorization for microendoscopic data (CNMF-E) packages[19, 20]. CaImAn isolates the cell components using matrix factorization and is dependent on an initialization step identifying locations for signal extraction, also known as seed points. Multiple methods are offered to identify seed points, for this work *GreedyCorr* introduced by Zhou et al. was implemented[21]. Briefly, a local correlation image and peak signal-to-noise ratio (PSNR) image are calculated from the temporal image stack ($\sigma = 10$ for local correlation). A point-wise product is then produced from these two images and segmented, identifying suitable locations for seed points.

The segmenting thresholds were previously optimized for colon epithelial calcium imaging to be 0.8 for local correlation and 5 for PSNR. The identified seed points were then used to iteratively fit the CNMF model to the temporal image stack, as outlined by Zhou et al., until the components reach a stabilized residual sum of squares (RSS)[21]. The output components for the CNMF model included isolated cell areas, isolated fluorescent profiles, and a background noise component. The cell areas and associated fluorescent profiles were then manually inspected, removing any misidentified or non-adherent cells. The final fluorescent profiles were then processed to identify calcium oscillations or spikes in a custom MATLAB script. Each signal was analyzed using the findpeaks command from the MATLAB image analysis toolbox using a peak threshold three times the signal's standard deviation and a search window of 5 seconds. The output signals and their associated peaks were inspected manually to identify misidentifications. The sum peaks were then calculated for each signal, and the pulse width for each peak was calculated using the output data from the findpeaks command.

3.2.8 EdU & KRT-20 staining and quantification

Prior to imaging epithelial cell colonies or patches (n=3 for each culture condition), the cells were pulsed with 10 μM 5-thynyl-2'-deoxyuridine (EdU, A10044, ThermoFisher Scientific) for 3 hours at 37 °C. After imaging, the cells were returned to the incubators and remained at 37 °C for 3 hours after EdU addition. The wells were then washed with 1x PBS, fixed with 5% paraformaldehyde for 15 minutes, washed with 3% bovine serum albumin (BSA In PBS and permeabilized with 0.5% Triton-X for 20 minutes, all at 25 °C. The cells were then washed twice in 3% BSA in PBS, followed by addition of 250 μL of EdU staining solution (with fluorophore) and incubated while protected from the light for 60 minutes at 25 °C. After a single wash with 1x PBS, fixative quenching was performed rinsing three times with 0.75% (w/v)

glycine/PBS solution (≥5 minutes for each). Thereafter, blocking was performed with 10% donkey serum in immunofluorescent buffer for 90 minutes at 25 °C prior to primary antibody incubation for 16 hours at 4 °C. The primary antibody chosen for the identification of differentiated colon cells was keratin-20 rabbit mAb (KRT20, 13063 Cell Signaling Technology), used at a dilution of 1:500. Wells were then rinsed with 1x PBS and incubated with secondary antibody AlexaFluor 488, anti-rabbit antibody (711-545-152, Jackson Immunoresearch, West Grove, PA) for 45 minutes at 25 °C protected from light. Afterward wells were rinsed with 1x PBS and incubated with 2 μg/mL Hoechst 3342 for 30 minutes at 25 °C protected from light. Wells were then rinsed with 1x PBS and two to three drops of glycerol were added to each well. Collagen scaffolds were then separated from the based of the culture wells and transferred to a glass slide for imaging. Imaging was performed on a Fluoview 3000 confocal microscope utilizing a 4x objective (0.16 NA, UPLSAPO) and 20x objective (0.45 NA, LUCPLFLN) for single cell analysis (Both Olympus Corporation, Tokyo, Japan). Fluorophore excitation was achieved with 405 nm, 488 nm, and 640 nm laser diodes, and emission fluorescence collected at 430-470 nm, 505-545 nm, and 650-750 nm wavelengths respectively. Z-stacks were collected at 4x spanning the entire monolayer and 20x at manually defined regions of interests (ROIs) using software optimized step sizes. If imaging did not occur the same day, cells were stored at 4 °C overnight protected from light in PBS containing 0.1% sodium azide. For image analysis, summed images for each z-stack was fed into a custom MATLAB script. Briefly, fluorescent images were intensity thresholded using a global threshold for each channel determined using the Triangle algorithm[22]. The percent area for each stain was then quantified, with EdU and KRT20 normalized to Hoechst 33342.

3.2.9 Statistical Analysis

Graphpad Prism 8.3 was used for all statistical analysis (GraphPad Software, Inc. La Jolla, CA). Multi comparisons were performed using a one-way ANOVA and Tukey's test. All statistical tests were performed at the 5% significance levels. Measurements are reported as the ± the standard deviation unless otherwise noted. For all statistical comparisons, p values are represented following the American Psychological Association (APA) style[23] of * for $p< 0.05$, ** for $p<0.01$, and *** for $p<0.001$.

3.3 Results and Discussion

3.3.1 Impact of growth factors on intracellular calcium signaling

Investigations were made into the impact of growth factors on the spatial-temporal characteristics of Ca^{2+} signaling in primary colon cells. A complex gradient of growth factors, receptors, and extracellular matrices exists along the colon crypt axis and govern the proliferation and differentiation along the crypt axis. Canonical Wnt signaling and Notch signaling pathways have been identified as key contributors in ISC maintenance and proliferation at the base of the colon crypt. As demonstrated by Miyoshi and Steppenbeck, the addition of Wnt3a and R-spondin, a potent coactivator of canonical Wnt signaling, to the culture media support a large population of intestinal stem cells[24]. Notch signaling works in unison with Wnt signaling, cell progenitors favoring secretory cell fates when reduced[3]. To investigate the impact of these growth factors on Ca^{2+} signaling, primary colon cells were prepared on neutralized collagen scaffolds and kept in expansion media for the first 48 hours post passage. They were then either resupplied with expansion media or differentiation media lacking Wnt3a, R-spondin, and Noggin for the following 48 hours. To investigate Notch signaling, a y-secretase inhibitor,

10mM DAPT was included in expansion media. At this point calcium imaging was performed and the signals isolated for spatial-temporal analysis. The colon cells which continued in expansion media had a significantly higher mean peak count of 5.1 ± 1.0 peaks over 12 minutes compared to 2.9 ± 0.4 peaks over 12 minutes in cells in differentiation media (Figure 3.1, EM: 13 signals, DM: 20 signals). An inverse shift is shown in the mean pulse width, the mean pulse width of signals from cells kept in expansion media being 24.3 ± 2.0 seconds and significantly lower than the 59.1 ± 8.4 seconds of cells in differentiation medium. The inhibition of Notch signaling shows a similar impact on Ca^{2+} signaling with a significant ($p<0.01$) decrease in oscillations to 2.85 ± 2.6 mean pulses over 12 minutes and a significant ($p<0.001$) increase in mean pulse width to 58.28 ± 40.9 seconds (DAPT: 13 signals). Cell proliferative capacity and differentiation status of the colon cells were then quantified using EdU and KRT20, normalizing the total area of each to the total area of Hoechst stained nuclei (Figure 3.5, n = 3 separate culture wells). The lack of L-WRN and Notch signaling showed a significant decrease on EdU area ratio, with 0.53 ± 0.15 in expansion media versus 0.03 ± 0.01 without L-WRN and 0.26 ± 0.05 in 10 mM DAPT. A significant inverse impact was present in the ratio of differentiated cells, 0.10 ± 0.17 in expansion media versus 0.31 ± 0.18 without L-WRN and 0.81 ± 0.19 with DAPT (DM: $p<0.001$, DAPT: $p<0.01$). Reviewing the results, a significant decrease in Ca^{2+} oscillations and an increase in pulse width showed a correlation with increased differentiation. These findings are in line with those found by Deng et al. in the drosophila model, showing increased cumulative cytosolic Ca^{2+} leading to epithelial growth[11].

The Wnt signaling pathway was investigated further, altering the concentration of available growth factors and using the chemical compound CHIR-99021 for conical Wnt pathway activation. CHIR-99021 is a glycogen synthesis kinase 3ß (GSK3ß) inhibitor and shown to

increase the proliferation of Lgr5+ ISCs[25, 26]. An optimal midpoint between proliferation and differentiation was first determined by titrating L-WRN and quantifying the ratio of proliferative cells. A dilution of 5% (v/v) L-WRN conditioned media in differentiation media was found as an acceptable midpoint between proliferation and differentiation, resulting in an EdU area ratio of 0.09 ± 0.04 normalized to Hoechst stained nuclei total area. Primary colon cells were prepared on neutralized collagen scaffolds (1mg/mL) and kept in EM for 48 hours, after which the concentration of L-WRN was reduced to 5% (v/v) for the following 48 hours with or without 2.5 μM CHIR-99021. Analyzing the spatial-temporal characteristics of the Ca^{2+} signaling showed CHIR-99021 had a significant impact on mean peak count compared to the 5% L-WRN control condition, 9.2 ± 4.3 versus 4.1 ± 3.8 mean peaks over 12 minutes, respectively (Figure 3.2 L-WRN: 12 signals, CHIR: 19 signals). A significant inverse relationship is seen in the mean pulse width for CHIR-99021 and 5% L-WRN, 24.3 ± 6.3 versus 50.3 ± 30.9 seconds respectively. The shift in Ca^{2+} signaling is not unexpected because of the previously identified association between decreased cytosolic Ca^{2+} and increased proliferation, however these results show a direct correlation with conical Wnt signaling. Wnt3a being at the highest relative concentration at the base of the colon crypt, suggests a decrease in Ca^{2+} oscillations and an increase in pulse width in ISCs and progenitors cells as they migrate upwards[1].

3.3.2 Luminal signaling

Investigations were made into the Ca^{2+} signaling pathways present in cells reflective of the differentiated cells along the luminal surface of the intestine. Multiple signals exist at the luminal end of the colon crypt, promoting differentiation and suppressing proliferation to maintain healthy intestinal homeostasis. Among these signals are bone-morphogenetic proteins that belong to the transforming growth factor-beta (TGF-ß) family which oppose Wnt-mediated self-

renewal and proliferation. BMP-2 and BMP-4 are most prevalent in the intestine, produced by mesenchymal cells, and through Smad-mediated transcription repression, suppress proliferation independent of Wnt signaling[4, 5]. The intestine is also host to multiple microbiota given rise to a vast array of metabolites[7]. Basal crypt cells are protected from these metabolites at the base of the colon crypt but endure increased exposure as they migrate upwards[9]. One of these metabolites, butyrate, has shown to be a potent inhibitor of intestinal stem/progenitor proliferation dependent on the Fox3 transcription factor[9]. To investigate the integration of these different signaling pathways, primary mouse colon cells were plated on neutralized collagen (1 mg/mL). The cells remained in expansion media for 48 hours, and then changed with the addition of either 1 mM butyrate, 10 ng/mL BMP-2, or 10 ng/mL BMP-9 in expansion media. BMP-9 has been shown to be a potent agonist with a high affinity for binding to activin receptor-line kinases 1 (ALK1)[27, 28]. After 48 hours of exposure, calcium imaging was performed and Ca^{2+} signals isolated for characterization. The isolated signals from BMP-2 and BMP-9 show a significant impact on the mean peak count, decreasing to a mean count of 1.60 ± 1.6 and 2.08 ± 1.8 peaks over 12 minutes, respectively (Figure 3.3, EM Ctrl: 29 signals, butyrate: 14 signals, BMP-2: 12 signals, BMP-9: 10 signals). Butyrate showed a similar impact, decreasing the mean peak count to 2.00 ± 1.8 peaks over 12 minutes. Besides the decrease in oscillations an inverse impact is identified for pulse widths with a mean pulse width of 37.01 ± 19.4, 37.18 ± 33.6, and 45.58 ± 32.14 seconds for BMP-2, BMP-9 and butyrate. Cell proliferative capacity and differentiation status of the colon cells were then quantified using EdU and KRT20, normalizing the total area of each to the total area of Hoechst stained nuclei (Figure 3.5). Both the BMPs and butyrate had a significantly decreased ($p<0.001$) EdU area ratio to 0.02 ± 0.01, 0.06 ± 0.01 and 0.11 ± 0.07 for BMP-2, BMP-9 and butyrate, respectively. Butyrate and BMP-9 showed a

significant ($p<0.001$) increase in KRT20 area ratio with 1.25 ± 0.92 and 1.21 ± 0.35, respectively. BMP-2 showed a less drastic but still significant ($p<0.01$) increase in differentiation with a KRT20 area ratio of 0.31 ± 0.31. Activating signaling pathways prominent at the luminal end of the colon crypt showed a significant impact to Ca^{2+} signaling even in with the presence of L-WRN. The overall impact was a decrease in oscillation frequency and the broadening of the average pulse width. These findings are still in line with previous findings in drosophila and show a correlation between elevated cumulative cytosolic Ca^{2+} and differentiation.

3.3.3 Dietary compounds

A sample of naturally occurring compounds were screened for their impact on Ca^{2+} signaling within primary colon cells. An advantage of in vitro colon culture systems is the rapid screening of drug and dietary compounds, as demonstrated by Wang et al. investigating the impact of 77 naturally occurring compounds proliferation and differentiation[16]. Compounds from the previously screened 77 compounds were chosen based on showing strong effects in either proliferation or differentiation (Table 3.1). Colon cells were seeded on neutralized collagen scaffolding (n=3 for each condition) and expanded for two days in EM, after which the media was changed, and L-WRN reduced to 5% (v/v) to make the impacts of the dietary compounds more apparent. Six separate compounds were added to the colon cell cultures at the noted concentration. After 48 hours of exposure to the dietary compounds, calcium imaging was performed, and signals isolated for characterization. Characterizing the isolated Ca^{2+} signals from the fluorescence image stacks revealed a significant ($p<0.01$) decrease in total oscillations for all dietary compounds, except glucotropaeolin, compared to the 5% L-WRN control condition. The average pulse width was not as drastic, with only matairesinol and ecalyptol

showing a significant ($p<0.001$) increase from the 5% L-WRN condition. The decreased oscillations and elevated pulse widths are not unexpected in response to punicalagin and ecalyptol, due to their implication in increased differentiation shown in primary mouse colon cells [16]. Based on their previous association with elevated proliferation, the decreased oscillations in response to isorhamnetin, N-nitrosoanabasine, and matairesinol are unexpected. Without staining data confirming the proliferative capacity however, there is the possibility proliferation was promoted through a signaling pathway not involving Ca^{2+}. Interpretation of the results would have benefited from immunofluorescent staining in succession with the Ca^{2+} imaging and should be included in future work. Interestingly, glucotropaeolin was previously shown to be toxic to primary colon cells but showed no significant impact on the Ca^{2+} signaling.

3.3.4 Impact of extracellular matrix stiffness on intracellular calcium signals

Mechanical cues within the local environment of the colon crypt, such as matrix stiffness, have shown to aid in the guidance of ISC fates and therefore its impact on Ca^{2+} signaling was investigated. The mechanical properties that can impact the ISC fate include stiffness, shape, and adhesion. Previous work by Gjorevski et al. has shown optimal expansion of colon cells on a scaffold with a stiffness of 1.3 kPA[10]. When colon cells were culture on matrices either softer or stiffer than 1.3 kPa there was a significant decrease in colon cell expansion. To investigate the impact of surface stiffness on Ca^{2+} signaling primary colon cells, mouse colon cells were cultured on three different culture platforms. The first was directly on a polystyrene culture plate commonly used for cell culture and having a relative high stiffness of ~3 GPa[29]. The second was neutralized collagen that was then cross-linked, therefore increasing its stiffness to approximately 9.6 kPa[30]. As a control, colon cells were also cultured on neutralized collagen

with a previously recorded stiffness between 100 and 300 Pa[31]. Primary mouse colon cells were passaged onto either neutralized collagen, cross-linked neutralized collagen, or polystyrene and supplied with expansion media. Calcium imaging was performed 48 hours post passage and isolating the Ca^{2+} signals for characterization. The Ca^{2+} oscillations in the stiffer matrices, cross-linked collagen and polystyrene, significantly decreased ($p<0.001$) to 1.55 ± 1.1 and 1.6 ± 1.57 peaks over 12 minutes relative to those found in the softer neutralized collagen (Figure 3.7, neutralized collagen: 13 signals, cross-linked: 31 signals, polystyrene: 19 signals). No significant differences were observed between the pulse widths. Cell proliferative capacity and differentiation status of the colon cells were then quantified using EdU and KRT20, normalizing the total area of each to the total area of Hoechst stained nuclei (Figure 3.7). The neutralized collagen had the largest proliferative capacity with EdU area ratio of 0.52 ± 0.15 and significantly ($p<0.01$) higher than the cross-linked collagen's area ratio of 0.17 ± 0.10 and polystyrene's area ratio 0.18 ± 0.08 (n = 3 separate culture wells for each condition). The polystyrene culturing showed the highest differentiation ratio of 1.43 ± 0.03 and was significantly higher ($p<0.001$) than 0.13 ± 0.03 and 0.05 ± 0.15 KRT-20 area ratios for cross linked and neutralized collagen, respectively. There was no significant difference ($p=0.61$) between the KRT20 area ratios shown in cross-linked and neutralized collagen.

Cells utilize multiple signaling pathways to sense the compression of neighboring cells and the stiffness of the surrounding ECM through mechanotransduction. These pathways include Raw/MAPK, PI3K/Akt, RhoA/ROCK, Wnt/β-catenin and TGF-β pathways[32–34]. The key downstream mediator of these pathways has been determined to be transcriptional co-activators Yes-associated-protein 1 (YAP) and Transcriptional coactivator with PDZ-binding motif (TAZ)[35]. YAP/TAZ activity has been found to impact intestinal stem cell proliferation and

differentiation, with increased nuclear translocation YAP/TAZ associated with increased proliferation and vice versa[10]. Interestingly, elevated Ca^{2+} signaling has been shown to suppress YAP/TAZ by increasing its phosphorylation and preventing accumulation in the nucleus[36]. In the results presented here, it would suggest YAP/TAZ as the downstream target of the increased cumulative Ca^{2+} observed in the stiffer ECMs cross-linked collagen and polystyrene, increasing YAP/TAZ cytoplasmic translocation and therefore ISC differentiation. As for the upstream source of elevated cytosolic Ca^{2+}, there exist multiple possibilities including RhoA signaling pathway and mechanosensitive ion channels[37, 38].

3.4 Conclusions

Using the 2D colon monolayer and signal isolation pipeline, multiple colon crypt signaling factors were examined for their impact on Ca^{2+} signaling. Signal pathways prevalent at the base of the colon crypt, Wnt/β-catenin and Notch signaling, were associated with decreased the Ca^{2+} oscillation frequency and narrowed the pulse widths. These shifts in signaling resulted in a decrease cumulative cytosolic Ca^{2+} which has been associated with ISC self-renewal, and were confirmed experimentally with EdU uptake[11]. Neither Wnt/β-catenin nor Notch pathways have been directly associated with cytosolic Ca^{2+} oscillations, there is however another Wnt signaling branch dependent on Ca^{2+} as a secondary messenger. In the Wnt/calcium signaling pathway either Wnt4 or Wnt5a ligands bind to Frizzeled (Fz) G-protein receptors, activating phospholipase C (PLC), elevating inositol 1,4,5-triphosphate (IP3) which binds to IP3 receptors and releases Ca^{2+} into the cytosol from the endoplasmic reticulum[39]. The elevated concentration of cytosolic Ca^{2+} is sufficient to activate downstream targets including calcium calmodulin depend kinase II (CamKII), protein kinase C (PKC) or calcineurin (CaCN). Interestingly, Deng

et al. determined CaCN to be the downstream target of the elevated cytosolic Ca^{2+} in the *drosophila* model leading to increased proliferation[11].

Moving to an area of less self-renewal and higher differentiation at the luminal end of the colon crypt, the impact of BMP and butyrate were investigated. Both BMP-2 and butyrate have been shown to elevate cell differentiation through signaling pathways involving Ca^{2+}. BMP-2 elevated differentiation through SMAD/Akt/Ca^{2+} signaling pathways, and butyrate through the activation of calcium-sensitive protein kinase C (PKC)[40]. With the L-WRN conditioned media still present, Ca^{2+} signaling showed a significant decrease in oscillation frequency and a broadening of the pulse width, therefore increasing the cumulative cytosolic Ca^{2+}. This shift in signaling was also associated by elevated differentiation as shown by KRT20 immunofluorescent staining following calcium imaging. These findings suggest an association between higher frequency narrow Ca^{2+} signals with self-renewal and inversely between lower frequency wider Ca^{2+} signals with differentiation.

3.5 Figures

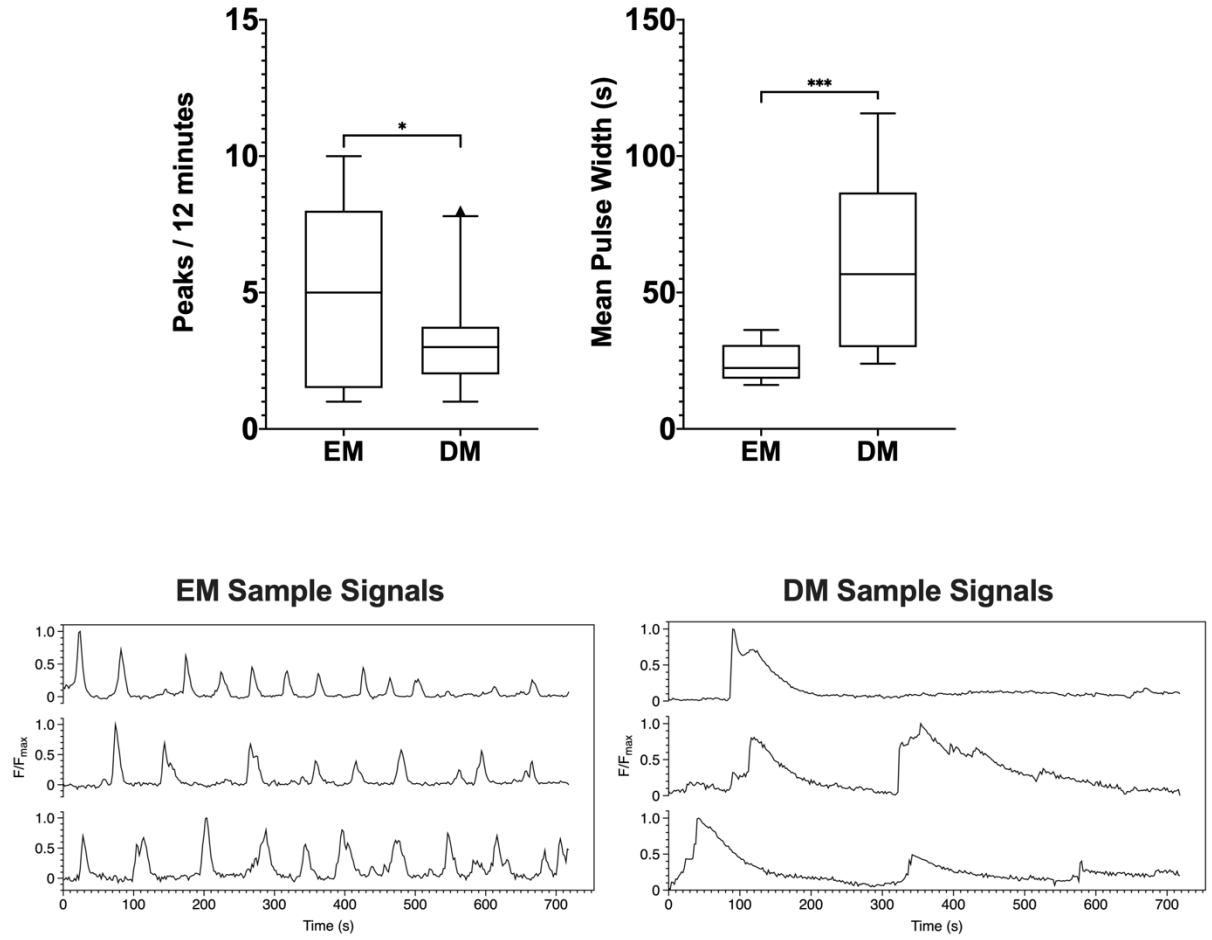

Figure 3.1 Box-and-whisker plot showing distributions of total Ca^{2+} oscillations over 12 minutes (top left) and mean pulse widths of Ca^{2+} signals (top right) after the removal of L-WRN conditioned media (DM). Boxes are centered on the median value and extend to the 25^{th} and 75^{th} percentiles. Whiskers extend to the 5^{th} and 95^{th} percentiles. The number of cell signals compared were 13 for EM and 20 for DM. Bottom row shows sample signals from each group (EM: left, DM: right) normalized to their max fluorescence.

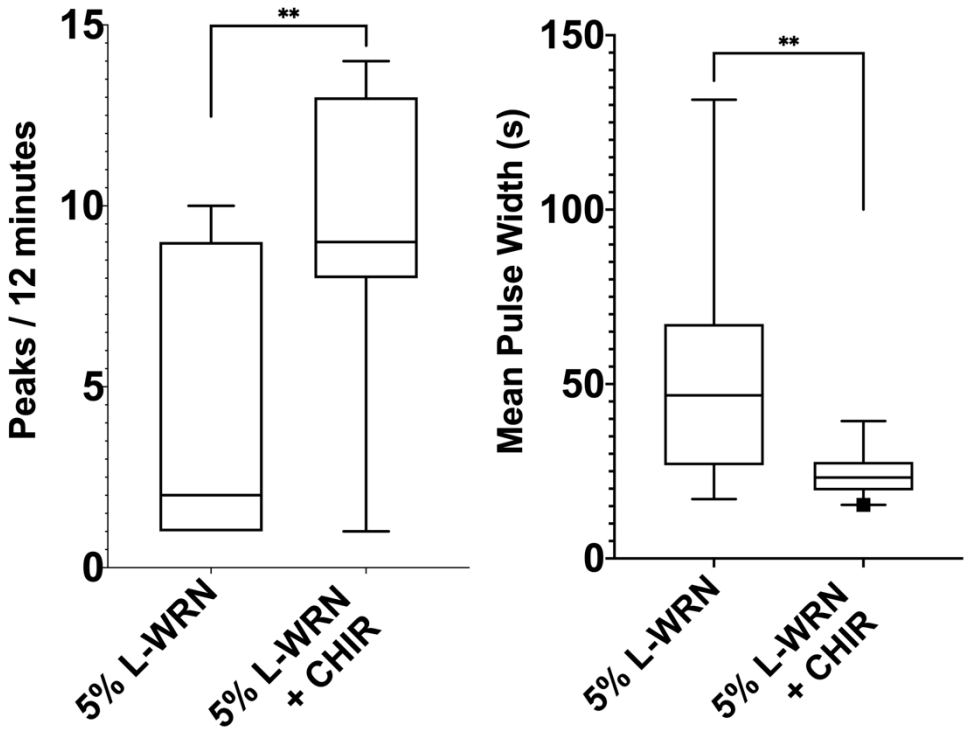

Figure 3.2 Box-and-whisker plot showing distributions of total Ca^{2+} oscillations over 12 minutes (left) and mean pulse widths of Ca^{2+} signals (right) with L-WRN conditioned media reduced to 5% (v/v) and addition of Wnt agonist CHIR-99021 (2.5 μM). Boxes are centered at the median and extend to the 25^{th} and 75^{th} percentiles. The whiskers extended to the 5^{th} and 95^{th} percentiles. The number of cell signals compared were 12 for 5% L-WRN and 19 for 5% L-WRN with CHIR-9901

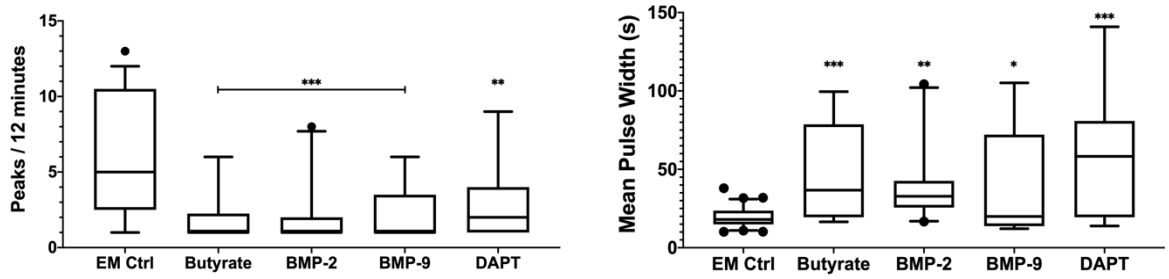

Figure 3.3 Box-and-whisker plot showing distributions of total Ca^{2+} oscillations over 12 minutes (left) and mean pulse widths (right) of Ca^{2+} signals in response to activation of differentiation signaling pathways and suppression of Notch signaling. Boxes are centered at the median and extend to the 25^{th} and 75^{th} percentiles, while the whiskers extend to the 5^{th} and 95^{th} percentiles. All significant differences shown are in comparison to EM control using Tukey's test for multi-comparison. The total number of cell signals compared for each condition were 29 for EM Ctrl, 14 for butyrate, 20 for BMP-2, 12 for BMP-9, and 13 for DAPT.

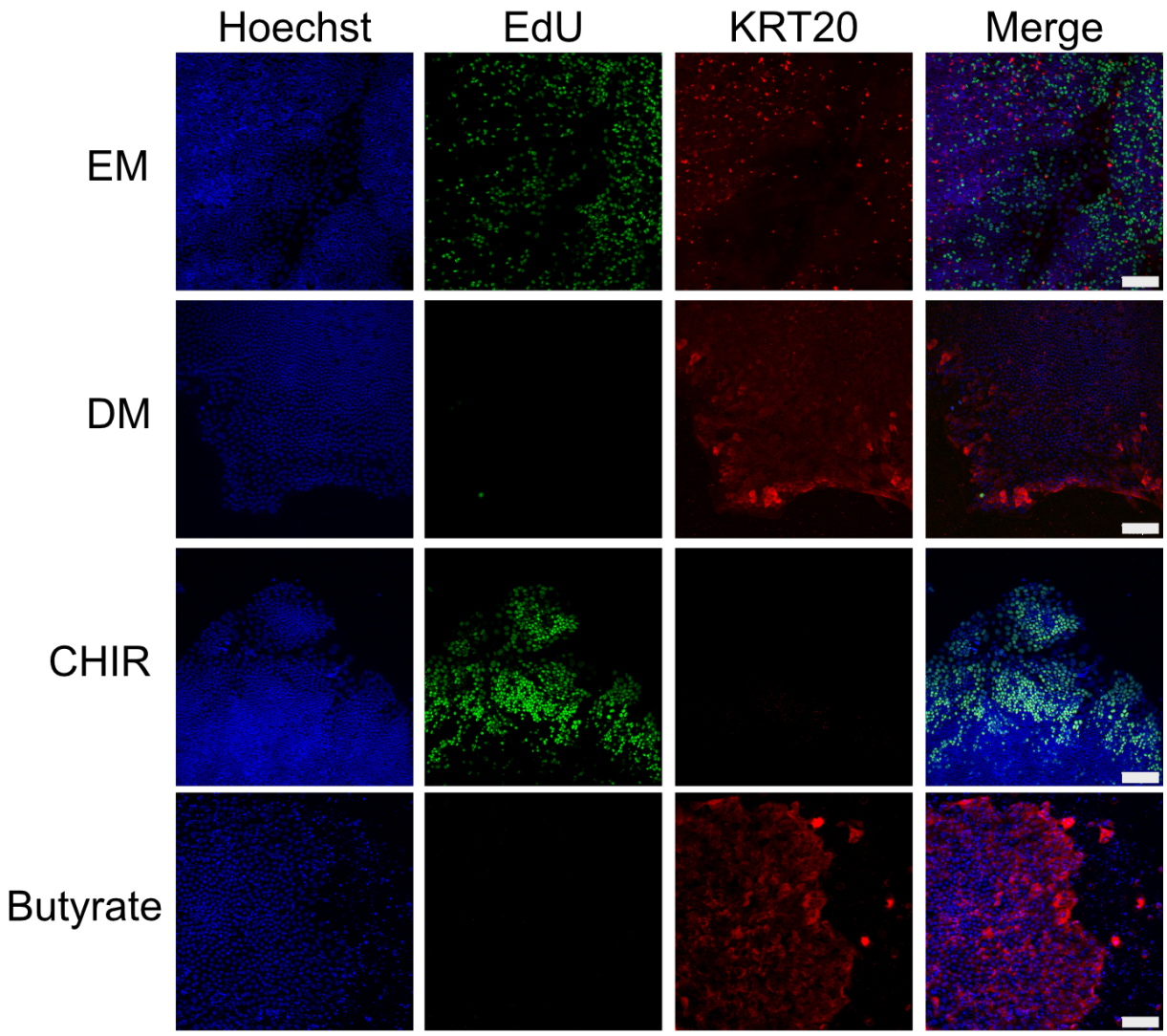

Figure 3.4 Fluorescent images of Hoechst, EdU incorporation, and cytoplasmic protein keratin-20 (KRT20). All scale bars are 100 μm.

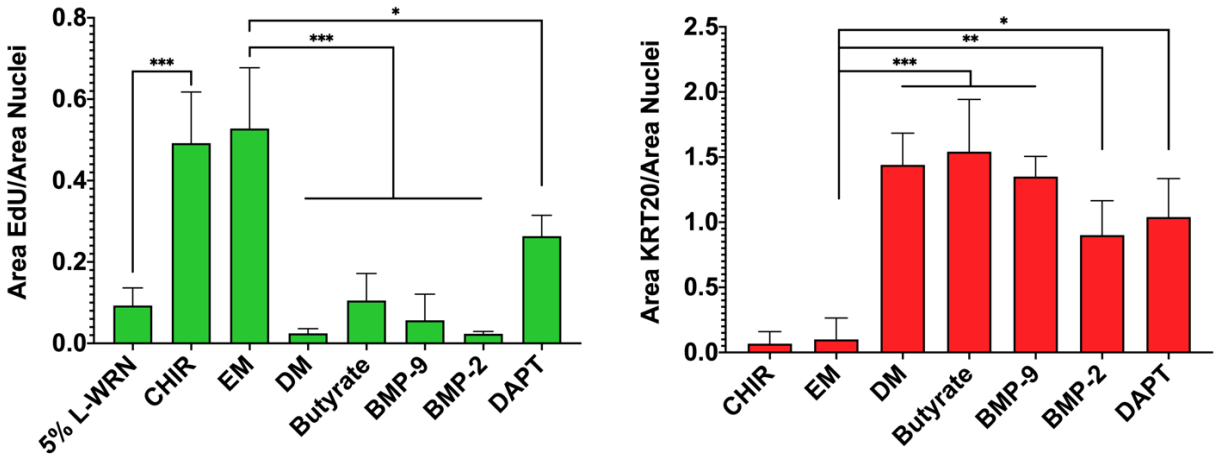

Figure 3.5 Quantification of EdU uptake for proliferative capacity and cytoplasmic protein Keratin-20 for differentiation status. The EdU and KRT20 area above the empirically determined threshold was normalized to the nuclear area (Hoechst-3342) and error bars represent standard deviation (n = 3 separate culture wells for each condition).

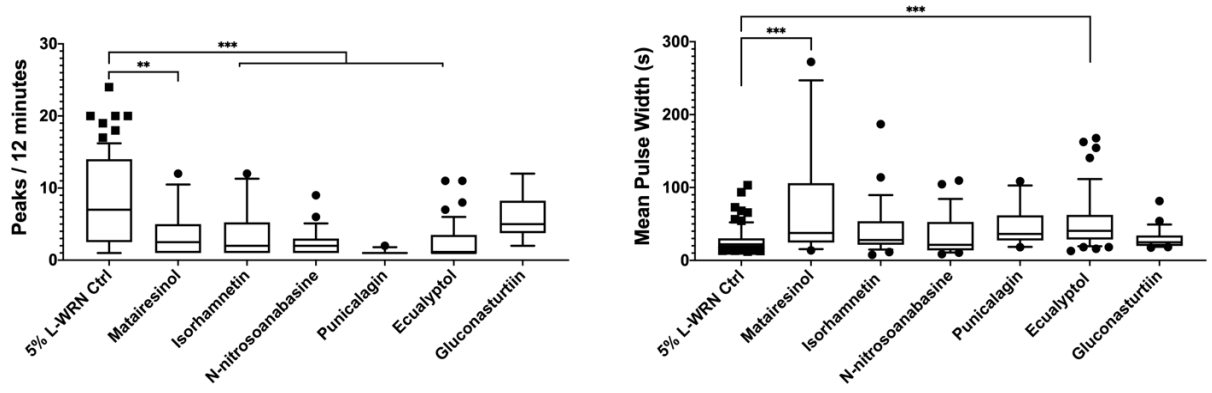

Figure 3.6 Box-and-whisker plot showing distributions of total Ca^{2+} oscillations over 12 minutes (left) and mean pulse widths (right) of Ca^{2+} signals collected following 48 hours exposure to a given dietary compound. Boxes are centered at median and extend to the 25^{th} and 75^{th} percentiles. Whiskers extended to the 5^{th} and 95^{th} percentiles. Total cell signals collected for each compound were 77 for 5% L-WRN control, 22 for matairesino, 15 for isorhamnetin, 28 for N-nitrosoanabasine, 11 for punicalagin, 49 for ecualyptol, and 14 for gluconasturtiin.

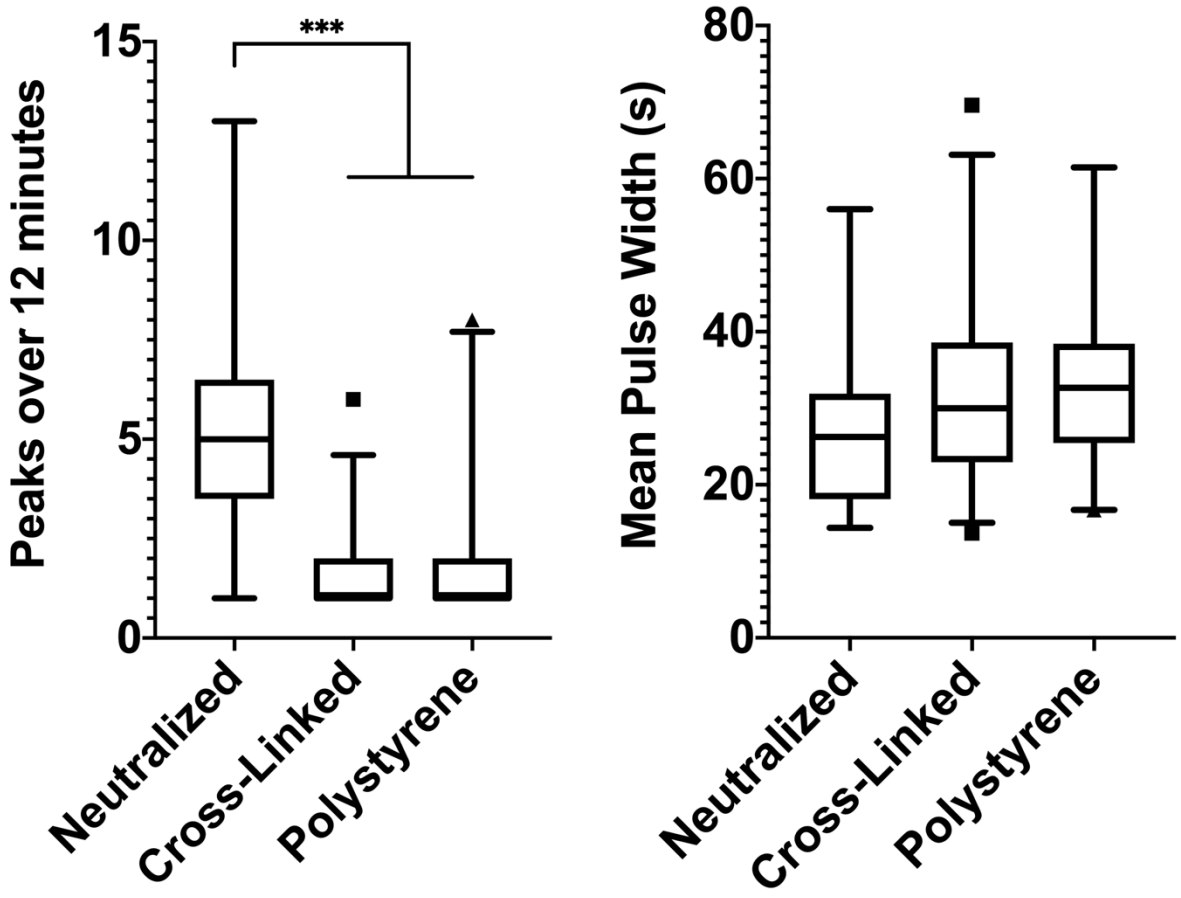

Figure 3.7 Box-and-whisker plot showing distributions of total Ca^{2+} oscillations over 12 minutes (left) and mean pulse width (right) of Ca^{2+} signals collected on different culture ECMs following 48 hours. The box is centered at the median value and extends to the 25^{th} and 75^{th} percentiles. Whiskers extend to the 10^{th} and 90^{th} percentiles. Total cell Ca^{2+} signals compared were 13 for neutralized collagen, 31 for cross-linked collagen, and 19 for polystyrene.

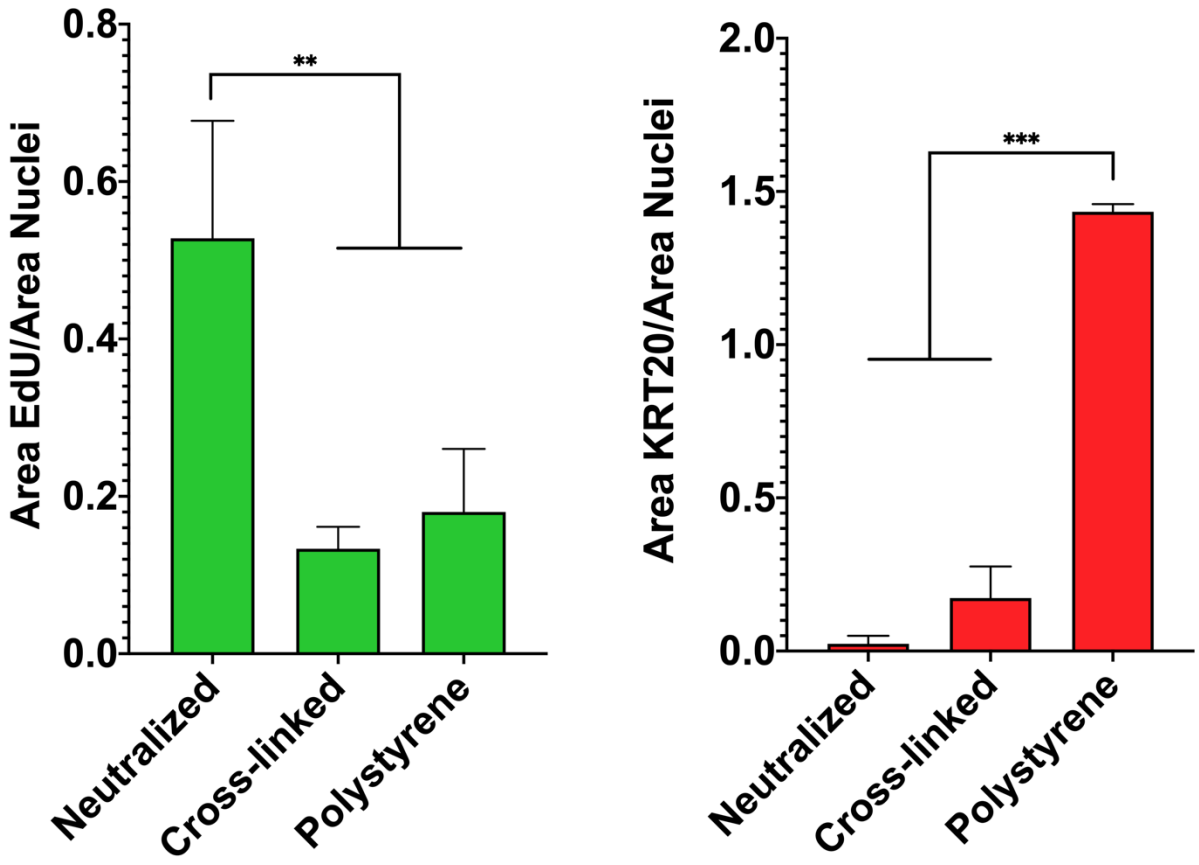

Figure 3.7 Quantification of EdU uptake for proliferative capacity and cytoplasmic protein Keratin-20 for differentiation status normalized to the nuclear area (Hoechst-3342). Primary colon cells were passaged onto the listed ECM in a 24-well plate and kept in EM for 48 hours. Error bars represent standard deviation (n = 3 separate culture wells for each condition).

3.6 Tables

Table 3.1 List of dietary compounds and natural products with their study concentration

Compound	Category	Study Concentration
Isorhamnetin[41]	Flavenoid	0.50 mM
Punicalagin[42]	Phenol	0.10 mM
Eucalyptol[43]	Terpenoid	1.00 mM
N-nitrosoanabasine[44]	Nitrate - Nitrosamine	1.00 mM
Glucotropaeolin isothiocyanate[45]	Nitrate - Glucosinolate	6.00 mM
Matairesinol[46]	Plant Lignan	0.05 mM

REFERENCES

1. Wang Y, Kim R, Hinman SS, Zwarycz B, Magness ST, Allbritton NL. Bioengineered Systems and Designer Matrices That Recapitulate the Intestinal Stem Cell Niche. Cmgh. 2018;5:440-453.e1.

2. Pinto D, Gregorieff A, Begthel H, Clevers H. Canonical Wnt signals are essential for homeostasis of the intestinal epithelium. Genes Dev. 2003;17:1709-1713.

3. VanDussen KL, Carulli AJ, Keeley TM et al. Notch signaling modulates proliferation and differentiation of intestinal crypt base columnar stem cells. Development. 2012;139:488-497.

4. Haramis APG. Erratum: De novo crypt formation and juvenile polyposis on BMP inhibition in mouse intestine (Science (March 12) (1684)). Science. 2004;304:1449.

5. Qi Z, Li Y, Zhao B et al. BMP restricts stemness of intestinal $Lgr5^{+}$ stem cells by directly suppressing their signature genes. Nat Commun. 2017;8:13824.

6. Qin J, Li R, Raes J et al. A human gut microbial gene catalogue established by metagenomic sequencing. Nature. 2010;464:59-65.

7. Matsumoto M, Kibe R, Ooga T et al. Impact of Intestinal Microbiota on Intestinal Luminal Metabolome. Scientific Reports. 2012;2

8. Sridharan GV, Choi K, Klemashevich C et al. Prediction and quantification of bioactive microbiota metabolites in the mouse gut. Nat Commun. 2014;5:5492.

9. Kaiko GE, Ryu SH, Koues OI et al. The Colonic Crypt Protects Stem Cells from Microbiota-Derived Metabolites. Cell. 2016;167:1137.

10. Gjorevski N, Sachs N, Manfrin A et al. Designer matrices for intestinal stem cell and organoid culture. Nature. 2016;539:560-564.

11. Deng H, Gerencser AA, Jasper H. Signal integration by Ca(2+) regulates intestinal stem-cell activity. Nature. 2015;528:212-217.

12. Nászai M, Carroll LR, Cordero JB. Intestinal stem cell proliferation and epithelial homeostasis in the adult Drosophila midgut. Insect Biochem Mol Biol. 2015;67:9-14.

13. George L. Calcium signalling in human colonic epithelium. In press 2019.

14. Yamazaki D, Hasegawa A, Funato Y et al. Cnnm4 deficiency suppresses Ca^{2+} signaling and promotes cell proliferation in the colon epithelia. Oncogene. 2019;38:3962-3969.

15. de Jong PR, Takahashi N, Harris AR et al. Ion channel TRPV1-dependent activation of PTP1B suppresses EGFR-associated intestinal tumorigenesis. J Clin Invest. 2014;124:3793-3806.

16. Wang Y, DiSalvo M, Gunasekara DB et al. Self-renewing Monolayer of Primary Colonic or Rectal Epithelial Cells. Cmgh. 2017;4:165-182.e7.

17. Miyoshi H, Stappenbeck TS. In vitro expansion and genetic modification of gastrointestinal stem cells in spheroid culture. Nat Protoc. 2013;8:2471-2482.

18. DiSalvo M, Harris DM, Kantesaria S et al. Characterization of Tensioned PDMS Membranes for Imaging Cytometry on Microraft Arrays. Anal Chem. 2018;90:4792-4800.

19. Giovannucci A, Friedrich J, Gunn P et al. CaImAn: An open source tool for scalable Calcium Imaging data Analysis. bioRxiv. 2018339564.

20. Giovannucci A, Friedrich J, Deverett B, Staneva V, Chklovskii DB, Pnevmatikakis EA. CaImAn-MATLAB version 6bd51e2. GitHub

21. Zhou P, Resendez SL, Rodriguez-Romaguera J et al. Efficient and accurate extraction of in vivo calcium signals from microendoscopic video data. Elife. 2018;7

22. Zack GW, Rogers WE, Latt SA. Automatic measurement of sister chromatid exchange frequency. Journal of Histochemistry and Cytochemistry. 1977;25:741-753.

23. American PA, others. Publication manual of the American psychological association Washington. DC: American Psychological Association. 2010

24. Miyoshi H, Stappenbeck TS. In vitro expansion and genetic modification of gastrointestinal stem cells in spheroid culture. Nature Protocols. 2013;8:2471-2482.

25. Yin X, Farin HF, van Es JH, Clevers H, Langer R, Karp JM. Niche-independent high-purity cultures of Lgr5+ intestinal stem cells and their progeny. Nat Methods. 2014;11:106-112.

26. Wang F, Scoville D, He XC et al. Isolation and characterization of intestinal stem cells based on surface marker combinations and colony-formation assay. Gastroenterology. 2013;145:383-95.e1.

27. Truksa J, Peng H, Lee P, Beutler E. Bone morphogenetic proteins 2, 4, and 9 stimulate murine hepcidin 1 expression independently of Hfe, transferrin receptor 2 (Tfr2), and IL-6. Proceedings of the National Academy of Sciences of the United States of America. 2006;103:10289-10293.

28. Kang Q, Sun MH, Cheng H et al. Characterization of the distinct orthotopic bone-forming activity of 14 BMPs using recombinant adenovirus-mediated gene delivery. Gene Therapy. 2004;11:1312-1320.

29. Callister WD, others. Fundamentals of materials science and engineering. Wiley London; 2000

30. Wang Y, Gunasekara DB, Reed MI et al. A microengineered collagen scaffold for generating a polarized crypt-villus architecture of human small intestinal epithelium. 201844-55.

31. Joshi J, Mahajan G, Kothapalli CR. Three-dimensional collagenous niche and azacytidine selectively promote time-dependent cardiomyogenesis from human bone marrow-derived MSC spheroids. Biotechnol Bioeng. 2018;115:2013-2026.

32. Halder G, Dupont S, Piccolo S. Transduction of mechanical and cytoskeletal cues by YAP and TAZ. Nature Reviews Molecular Cell Biology. 2012;13:591-600.

33. Sun Y, Chen CS, Fu J. Forcing Stem Cells to Behave: A Biophysical Perspective of the Cellular Microenvironment. Annual Review of Biophysics. 2012;41:519-542.

34. Dupont S, Morsut L, Aragona M et al. Role of YAP/TAZ in mechanotransduction. Nature. 2011;474:179-184.

35. Boopathy GTK, Hong W. Role of Hippo Pathway-YAP/TAZ signaling in angiogenesis. Frontiers in Cell and Developmental Biology. 2019;7:1-12.

36. Liu Z, Wei Y, Zhang L et al. Oncogene Induction of store-operated calcium entry (SOCE) suppresses glioblastoma growth by inhibiting the Hippo pathway transcriptional coactivators YAP/TAZ. 2019:120–139.

37. Kim TJ, Seong J, Ouyang M et al. Substrate rigidity regulates Ca2+ oscillation via RhoA pathway in stem cells. Journal of Cellular Physiology. 2009;218:285-293.

38. Kobayashi T, Sokabe M. Sensing substrate rigidity by mechanosensitive ion channels with stress fibers and focal adhesions. Current Opinion in Cell Biology. 2010;22:669-676.

39. De A. Wnt/Ca2+ signaling pathway: a brief overview. Acta biochimica et biophysica Sinica. 2011;43:745-756.

40. T. T, T. S, M. NN et al. Effect of MDR1 gene promoter methylation in patients with ulcerative colitis. International Journal of Molecular Medicine. 2009;23:521-527.

41. Duan J, Xie Y, Luo H, Li G, Wu T, Zhang T. Transport characteristics of isorhamnetin across intestinal Caco-2 cell monolayers and the effects of transporters on it. Food Chem Toxicol. 2014;66:313-320.

42. Lee SI, Kim BS, Kim KS, Lee S, Shin KS, Lim JS. Immune-suppressive activity of punicalagin via inhibition of NFAT activation. Biochem Biophys Res Commun. 2008;371:799-803.

43. Zhang W, Lim L-Y. Effects of Spice Constituents on P-Glycoprotein-Mediated Transport and CYP3A4-Mediated Metabolism in Vitro. Drug Metabolism and Disposition. 2008;36:1283-1290.

44. Liao J, Pan Y, Li C, Wen D, Liu H. Fast Screening for Tobacco-Specific N-nitrosamines by CZE Using Dynamically Coated Capillaries. Chromatographia. 2011;74:415-419.

45. Combourieu B, Elfoul L, Delort AM, Rabot S. Identification of new derivatives of sinigrin and glucotropaeolin produced by the human digestive microflora using 1H NMR spectroscopy analysis of in vitro incubations. Drug Metabolism and Disposition. 2001;29:1440-1445.

46. During A, Debouche C, Raas T, Larondelle Y. Among plant lignans, pinoresinol has the strongest antiinflammatory properties in human intestinal Caco-2 cells. J Nutr. 2012;142:1798-1805.

CHAPTER 4: CHARACTERIZATION OF CA^{2+} SIGNALING ON 2D CRYPT PLATFORM

4.1 Introduction

The colon epithelium undergoes constant self-renewal supported by rapidly dividing stem cells located at the base of invaginations into the underlying mesenchyme known as crypts[1]. Colon crypts act as a protective niche to support the stem cells which give rise to trans-amplifying cells that migrate upwards towards the luminal surface of the colon[2, 3]. The transition between cell proliferation and differentiation along the crypt's long axis is thought to be due to gradients in multiple biochemical and biophysical stimuli along the long-axis of the crypt *in vivo*[4, 5]. Wnt and Noggin, shown to promote proliferation, have the highest concentration at the base of the crypt and decrease in concentration towards the luminal crypt end[6]. While the differentiation factor, BMP, has an inverse concentration gradient with the highest concentration at the luminal surface[7]. Gradients are also presented in the ECM surrounding the colon crypts aiding in the promotion of proliferation or differentiation of colon cells[8].

Advancements in modeling the intestinal structural and mechanical properties have allowed for the study of primary colon tissue *in vitro*. Stem cells derived from the colonic epithelium can be cultured to form organoids or a self-renewing monolayer with addition of soluble growth factors such as Wnt-3A, R-spondin, and Noggin[9]. Although these *in vitro* models express the same cell types found *in vivo* and allow for long term colon cell culture, the models are limited and do not display the cell patterning found *in vivo* colon crypts. More recent *in vitro* models

have introduced biochemical and biophysical gradients to establish the compartmentalization of proliferative and differentiated colon cells. Primary murine colonoids demonstrated significant polarization when cultured on a specially designed microfluidic device under a linear gradient of Wnt-3A and R-spondin1[10]. Three-dimensional *in vitro* colon crypts have also been demonstrated, using a hydrogel scaffolding with micro-well dimensions resembling that of *in vivo* colon crypts[11–13]. In this system, a monolayer of primary colonic cells covers the microcell surface so that an array of 100 cell-covered wells is form on an approximately 1 mm-sized device. An advantage of this culture method over the organoid/colonoid models is the access to both the basal and luminal surfaces. Since this model incorporates both a luminal and basal fluid reservoir, a growth factor gradient can be established by supplying growth factors to the basal reservoir only. This limits the stem cell niche with its proliferative cells to the base of the microcells or *in vitro* colon crypts. Although these methods show great promise in modeling the polarization shown in colon crypts, they require advanced microscopy techniques to adequately interrogate their 3D architecture.

Recently, Raeyhun et al. demonstrated a novel platform mimicking *in vitro* the cell compartmentalization found in colon crypts with a two-dimensional monolayer of primary murine colon cells *i.e.* "flat crypts"[14]. The micro-devices consisted of an impermeable photoresist film patterned with a 10 x 10 array of microholes (50 μm dia.) separating a basal and luminal reservoir. A collagen layer coated the photoresist film as well as spanned across the microholes. Importantly the collagen layer was permeable to growth factors while the photoresist film was not. Primary colon epithelial cells grew as a monolayer across the collagen-coated photoresist as well as the thin collagen film spanning the holes[9]. Limiting growth factors to the basal reservoir, resulted in cell proliferation constrained to a 50 μm radius above the collagen-

covered microholes. These cells migrated outward from these proliferative centers becoming increasingly differentiated with further distance from the microhole center (>50μm) and growth factor source. Thus the collagen-coated microholes acted to provide a "stem cell niche" while the more distant regions acted to support a differentiated cell zone. Therefore, the 2D or flat crypt platform provides a high throughput colonic epithelial model for studying the impact of soluble growth factors and their gradient profiles on primary intestinal tissue.

This work aims to improve on previous investigations into colon cell calcium signaling through the implementation of the 2D colon crypt platform and its ability to produce distinct proliferative and differentiated cell zones that are readily visualized by standard microscopy. Limitations in previous experimental design included limited knowledge of the cell types within a cell patch during calcium imaging, potentially resulting in an inadequate sampling of all cell populations present. Previous experimentation also lacked biochemical and biophysical gradients found in colon crypts, being exposed to a fixed concentration of either growth or differentiation factors. The 2D crypt platform was modified for the measurement of Ca^{2+} signaling in murine colonic cells. This was accomplished by decreasing the thickness of photoresist film for improved imaging of Ca^{2+} indicator Cal-520. The cell compartmentalization provided by the 2D colon crypt platform allowed for focused investigations in areas of heightened proliferation above the microholes and the impact of decreased growth factors on outward migrating cells.

4.2 Materials and Methods

4.2.1 Microdevice fabrication

Photoresist films were fabricated with and without a sacrificial layer of PAA between the slide and photoresist film. When a polyacrylic acid (PAA) sacrificial coating on the glass surface

was utilized, a thin layer of PAA (30kDa, 30% in H_2O) was spin coated at 1500 rpm for 30 seconds. Glass slides with a PAA coating were dried for a minimum of two hours at 95 °C prior to use. Negative photoresist 1002F-10 was spin coated onto a glass side in 2-steps, first 550 rpm for 10 seconds followed by 1700 rpm for 30 seconds. Thereafter the glass slides were cured at 95 °C for 1 hour while protected from light. The negative photoresist was then exposed to ultraviolet light for a total energy of 600 mJ through a photomask with an array of open circles. The glass slides were then transported to the development area while light protected. Exposed photoresist was developed using propylene glycol methyl ether acetate (PGMEA) and then baked at 95 °C for 12 hours. Transwell cassettes were then firmly attached to the photopatterned photoresist film on the glass slides using 3M double-sided medical tape. The slide/cassette combination was then incubated in DI water at 70 °C for two hours to dissolve the PAA between the photoresist and glass slide. The glass sides were carefully detached from the photoresist film cutting away any excess film around the cassette base. If any difficulty in separating the film presented itself, slides were allowed to incubate further in water in one hour increments.

4.2.2 Cell culture media composition

Expansion media (EM) for cell culture contained advanced DMEM/F12 medium, L-WRN conditioned medium, HEPES (10 mM, pH 7.5), EGF (50 ng/mL), GlutaMAX (2 mM), priomcin (100 µg/mL), and Y-27632 ROCK inhibitor (10 µM). As previously outlined by Stappenbeck et al., L-WRN conditioned medium was prepared by the culturing of L-WRN cells (ATCC, #3276) and harvesting Wnt-3A, R-spondin 3, and noggin secreted into the supernatant by cells[15]. Wnt-3A, R-spondin 3, and noggin were used at final concentrations in the culture medium of 30, 75 and 71 ng/mL, respectively. Differentiation media (DM) contained DMEM/F12 medium,

HEPES (10mM, pH 7.5), GlutMAX (2 mM), primocin (100 µg/mL), N-acetylcysteine (1.23 mM), EGF (50 ng/mL), and A83-01 (500 nmol/mL).

4.2.3 Primary mouse colon culture

Murine large intestines were collected from both female and male mice between the ages of 6 and 10 weeks. The colonic crypts were isolated using a previously published protocol from the Allbritton group[9]. In summary, the intestinal tissue was cut longitudinally to expose the luminal and basal sides of tissue before being placed in ethylenediaminetetraacetic acid (EDTA, 2 mM) and dithiothretol (DTT, 0.5 mM) in buffer (5.6 mM Na2HPO4, etc.) for 90 minutes at room temperature. Through vigorous shaking the crypts/villi were dissociated and collected by centrifugation. Crypt density was measured using a 10 µL suspension on a petri dish and approximately 1000 crypts/cm^2 distributed per well in a 6-well plate. For the first 48-hours of culture Y-27632 was added to the medium to minimize apoptotic death. The culture media was changed every 48 hours after that. Once cell coverage reached 80% the wells were subcultured involving a 2-step dissociation method. Culture media was aspirated, the collagen scaffold separated from the well using 1-mL pipette tip and transferred to a 15-mL conical tube containing 1 mL of culture media and 500 U/mL of collagenase type IV. A 5-mL and then 1-mL pipette tip were used to mechanically breakdown the collagen further. The conical tube with cells was then incubated at 37°C for 10 minutes. After centrifugation at 600 x g for 1 minute, the cells were washed in 5 mL of 1x PBS. The cells were then further detached from their substrate by incubation in 150 µL EDTA (500 µmol/L), and Y-27632 (10 µmol/L), incubated at 37°C for 2 minutes. This was followed by pipetting 20 to 50 times with a 200 µL pipet tip to disperse the cells. The cells were resuspended in culture media and passaged a ratio of 1:3 onto fresh collagen scaffolds.

4.2.4 Calcium imaging and image analysis

Culture plates were placed in the tissue culture hood and culture media replaced with a calcium-indicator loading media, which consisted of the base media the cells were already in (*i.e.* expansion media or differentiation media) with 1% Pluronic-F127 and 2% Probenecid. Cal-520 AM was added to the media, at a concentration of 5 μM and the cells were returned to the incubator for a total of one hour. For the final 30 minutes of loading, Hoechst 33342 (0.16 μM) was included for cell counting. After incubation the cell plate was moved to a tissue culture hood, rinsed three times with 1x PBS and then supplied with fresh loading media. The plate was transferred to a custom insert on the microscope stage within a customized incubation chamber. During imaging the cells remain at 37°C and the surrounding atmosphere was at >40% humidity. A brightfield area scan of the cells was performed using the 4x objective (NA 0.6), with a 5% overlap between fields of view. An automated focus algorithm maintained the appropriate focal plane during imaging as previously described[16]. The images were then stitched together and higher magnification imaging sites selected based on cells identified over the collagen-covered holes. Brightfield imaging and Hoechst 33342 fluorescent imaging was performed at each site using the 40x objective (NA 0.13). Fluorescent images of the calcium indicator were collected for each site at 2 second time points (Gain 1, Binning 2) for a total of 12 minutes resulting in a temporal image stack of 360 images.

4.2.5 Image analysis

The collected calcium image stacks were first manually inspected to confirm image integrity and the presence of time-varying fluorescence or calcium signals. If fluorescence changes were identified in the image stack, the images were then fed into a cell isolation pipeline written in MATLAB utilizing the Calcium Image Analysis (CaImAn) and constrained non-

negative factorization for microendoscopic data (CNMF-E) packages[17, 18]. CaImAn isolates the cell components using matrix factorization and is dependent on an initialization step identifying locations for signal extraction, also known as seed points. Multiple methods are offered to identify seed points, for this work *GreedyCorr* introduced by Zhou et al. was implemented[19]. Briefly, a local correlation image and peak signal-to-noise ratio (PSNR) image are calculated from the temporal image stack ($\sigma = 10$ for local correlation). A point-wise product is then produced from these two images and segmented, identifying suitable locations for seed points. The segmenting thresholds were previously optimized for colon epithelial calcium imaging to be 0.8 for local correlation and 8 for PSNR. The identified seed points were then used to iteratively fit the CNMF model to the temporal image stack, as outlined by Zhou et al., until the components reach a stabilized residual sum of squares (RSS)[19]. The output components for the CNMF model included isolated cell areas, isolated fluorescent profiles, and a background noise component. The cell areas and associated fluorescent profiles were then manually inspected, removing any misidentified or non-adherent cells. The final fluorescent profiles were then processed to identify calcium oscillations or spikes in a custom MATLAB script. Each signal was analyzed using the findpeaks command from the MATLAB image analysis toolbox using a peak threshold three times the signal's standard deviation and a search window of 5 seconds. The output signals and their associated peaks were inspected manually to identify misidentifications. The sum peaks were then calculated for each signal, and the pulse width for each peak was calculated using the output data from the findpeaks command.

4.2.6 EdU & Krt-20 staining and quantification

Prior to imaging epithelial cell colonies or patches (n=3 for each culture condition), the cells were pulsed with 10 μM 5-thynyl-2'-deoxyuridine (EdU, A10044, ThermoFisher

Scientific) for 3 hours at 37 °C. After imaging, the cells were returned to the incubators and remained at 37 °C for 3 hours after EdU addition. The wells were then washed with 1x PBS, fixed with 5% paraformaldehyde for 15 minutes, washed with 3% bovine serum albumin (BSA In PBS and permeabilized with 0.5% Triton-X for 20 minutes, all at 25 °C. The cells were then washed twice in 3% BSA in PBS, followed by addition of 250 µL of EdU staining solution (with fluorophore) and incubated while protected from the light for 60 minutes at 25 °C. After a single wash with 1x PBS, fixative quenching was performed rinsing three times with 0.75% (w/v) glycine/PBS solution (≥5 minutes for each). Thereafter, blocking was performed with 10% donkey serum in immunofluorescent buffer for 90 minute at 25 °C prior to primary antibody incubation for 16 hours at 4 °C. The primary antibody chosen for the identification of differentiated colon cells was keratin-20 rabbit mAb (KRT20, 13063 Cell Signaling Technology), used at a dilution of 1:500. Wells were then rinsed with 1x PBS and incubated with secondary antibody AlexaFluor 488, anti-rabbit antibody (711-545-152, Jackson Immunoresearch, West Grove, PA) for 45 minutes at 25 °C protected from light. Afterward wells were rinsed with 1x PBS and incubated with 2 µg/mL Hoechst 3342 for 30 minute at 25 °C protected from light. Wells were then rinsed with 1x PBS and two to three drops of glycerol were added to each well. Collagen scaffolds were then separated from the based of the culture wells and transferred to a glass slide for imaging. Imaging was performed on a Fluoview 3000 confocal microscope utilizing a 4x objective (0.16 NA, UPLSAPO) and 20x objective (0.45 NA, LUCPLFLN) for single cell analysis (Both Olympus Corporation, Tokyo, Japan). Fluorophore excitation was achieved with 405 nm, 488 nm, and 640 nm laser diodes, and emission fluorescence collected at 430-470 nm, 505-545 nm, and 650-750 nm wavelengths respectively. Z-stacks were collected at 4x spanning the entire monolayer and 20x at manually defined regions

of interests (ROIs) using software optimized step sizes. If imaging did not occur the same day, cells were stored at 4 °C overnight protected from light in PBS containing 0.1% sodium azide. For image analysis, summed images for each z-stack was fed into a custom MATLAB script. Briefly, fluorescent images were intensity thresholded using a global threshold for each channel determined using the Triangle algorithm[20]. The percent area for each stain was then quantified, and the EdU and KRT20 areas were divided by the area positive for Hoechst 33342. This normalization was performed to account for the varying cell densities.

4.2.7 Statistical analysis

Graphpad Prism 8.3 was used for all statistical analysis (GraphPad Software, Inc. La Jolla, CA). Multi comparisons were performed using a one-way ANOVA and Tukey's test. All statistical tests were performed at the 5% significance levels. Measurements are reported as the ± the standard deviation unless otherwise noted. For all statistical comparisons, p values are represented following the American Psychological Association (APA) style[21] of * for $p< 0.05$, ** for $p<0.01$, and *** for $p<0.001$.

4.3 Results and Discussion

4.3.1 Microfabrication optimization

Modifications were made to the microfabricated device for improved calcium imaging of the 2D colon crypts. The negative photoresist 1002F was selected for its lower fluorescence and improved fabrication capabilities particularly decreased brittleness compared to another commonly used photoresist, SU-8[22]. A small amount of fluorescence is still emitted by 1002F resin at a wavelength of 540 nm when exited at 485 nm which posed a challenge for its combined application with the calcium indicator Cal-520. To minimize possible fluorescence and

absorption, 1002F-50 was replaced with 1002F-10 during film fabrication to reduce the photoresist film thickness to 10 microns (from approximately 50 microns). The decreased thickness lead to challenges in separating the film from its glass backing and attachment to its Transwell frame, often leading to a device failure rate greater than 80%. Multiple methods to improve separation were investigated. These included addition of a sacrificial PAA layer and increased incubation temperatures during film detachment and/or increased incubation times (Table 4.1). Although the PAA layer improved photoresist film separation (>87% successful separation for 32 devices), the resulting colon monolayer showed no polarization around the microholes (0%, n = 8 devices). The lack of polarization suggests the PAA layer interfered with the formation of the photopatterned microholes preventing growth factors from reaching the luminal reservoir. The optimal separation technique for 1002F-10 involved attaching the Transwell frame to the film prior to separation and incubating the combination in deionized water for four hours at 75 °C without the use of a PAA sacrificial layer. Using the previously published protocol by Raehyun et al., primary murine colon cells were seeded onto the microdevices for validation of colon cell culturing and polarization[14]. EM was provided to the luminal and basal reservoirs for 48 hours. Thereafter, a media change was performed switching the luminal reservoir to DM. To verify proliferative/differentiation zones, fluorescent imaging was performed with Hoechst-33342, EdU, and KRT20 (Figure 4.2). The fluorescent images were intensity thresholded using global thresholds for each fluorescent channel determined by the Triangle algorithm[20]. Radial profiles were calculated using the pixel value sum of concentric circles emanating from the microhole center at 5 μm intervals and divided by pixel count. The EdU and KRT20 radial profiles were then normalized to Hoechst area and showed increased proliferation within a 50 μm radius of the microhole (Figure 4.2, 4.3).

Inversely, KRT20 fluorescence indicating differentiated cells increased with distance from the microhole. Investigating possible reduction in signal-to-noise ratio (SNR) for calcium imaging showed no significant difference ($p = 0.294$) between the traditional neutralized scaffolding and the 2D crypt platform, which had mean SNRs of 17.6 ± 3.6 and 16.6 ± 3.7 respectively ($n = 40$ and 26 Ca^{2+} signals). These results show polarization similar to that previously obtained using thicker photoresist films fabricated from 1002F-50, with 10 μm films fabricated using 1002F-10.

4.3.2 Spatial-temporal signal characteristics

Isolated Ca^{2+} signals were characterized above and near the microholes connecting the basal reservoir. These holes are the only source for the growth factors ˆWnt3a, Noggin, and R-spondin, resulting in a higher cell proliferation near the center of the holes as shown in earlier work[14]. Primary murine colon cells were cultured on the microdevice, with EM in the basal and luminal reservoirs for 48 hours. Thereafter, a media change was performed for each reservoir replacing the luminal media with DM. After another 48 hours, calcium imaging was performed on the colon cells, followed by staining for EdU incorporation and the presence of KRT20. Isolating the imaged Ca^{2+} signals and characterizing them resulted in a heterogenous mix of spatial-temporal properties. When the fluorescence of the Ca2+ indicator was imaged over time, the measured signals were heterogenous in their spatial-temporal properties. Signals were grouped based on their distance from the nearest microhole center, either within a 50 μm radius from the center or between 50 and 100 μm from the center. As expected, the signals near the microhole showed significantly higher ($p<0.001$) oscillation frequency compared to those further away, 3.3 ± 1.4 versus 1.2 ± 0.4 average oscillations over 12 minutes (Figure 4.4). An inverse relationship was observed in the pulse width, the average pulse width measured 45.4 ± 14.4 seconds within 50 μm of the microhole center compared to 78.1 ± 49.2 seconds located further

than 50 μm from the hole center. These results agree with the earlier studies involving elevated Wnt3a, Noggin and R-spondin concentrations resulting in a higher frequency of narrower Ca^{2+} oscillations.

4.4 Conclusions

Investigations into colon crypt Ca^{2+} signaling was continued on the 2D colon crypt system which contains distinct proliferative and differentiated cell zones. A challenge in the prior work included limited knowledge of the cell types during calcium imaging. The 2D crypt system was optimized for use with Ca^{2+} indicator Cal-520, replacing the 1002F-50 photoresist with 1002F-10 and reducing the thickness of the photoresist film to 10 μm. The successful formation of 2D crypts and measurement of Ca^{2+} signals in the epithelial monolayer showed no significant reduction in SNR ($p = 2.94$) compared to the transparent neutral collagen scaffold. Furthermore, successful polarization was achieved through the limitation of soluble growth factors to the basal reservoir and the characterization of Ca^{2+} signaling along a growth factor gradient (from hole center to inter-hole regions). As expected, Ca^{2+} oscillations from colon cells experiencing a higher concentration of soluble growth factors near the microholes (<50 μm) occurred at a higher frequency in narrow pulses. Moving further from the microhole holes (>50 μm), into areas of greater differentiation, resulted in the Ca^{2+} signals broadening and decreasing in frequency. These findings support the correlation between heightened colon cell proliferation and decreased cytosolic Ca^{2+}, and the inverse relationship of decreased proliferation and increase cytosolic Ca^{2+}. Interestingly, Ca^{2+} signaling was not found further than 84 μm from the center of the nearest microhole suggesting a decrease in cytosolic Ca^{2+} signaling in differentiated colon cells.

Future work on these devices is currently ongoing in the Allbritton lab involving methods for improved separation and different microhole patterns.

4.5 Figures

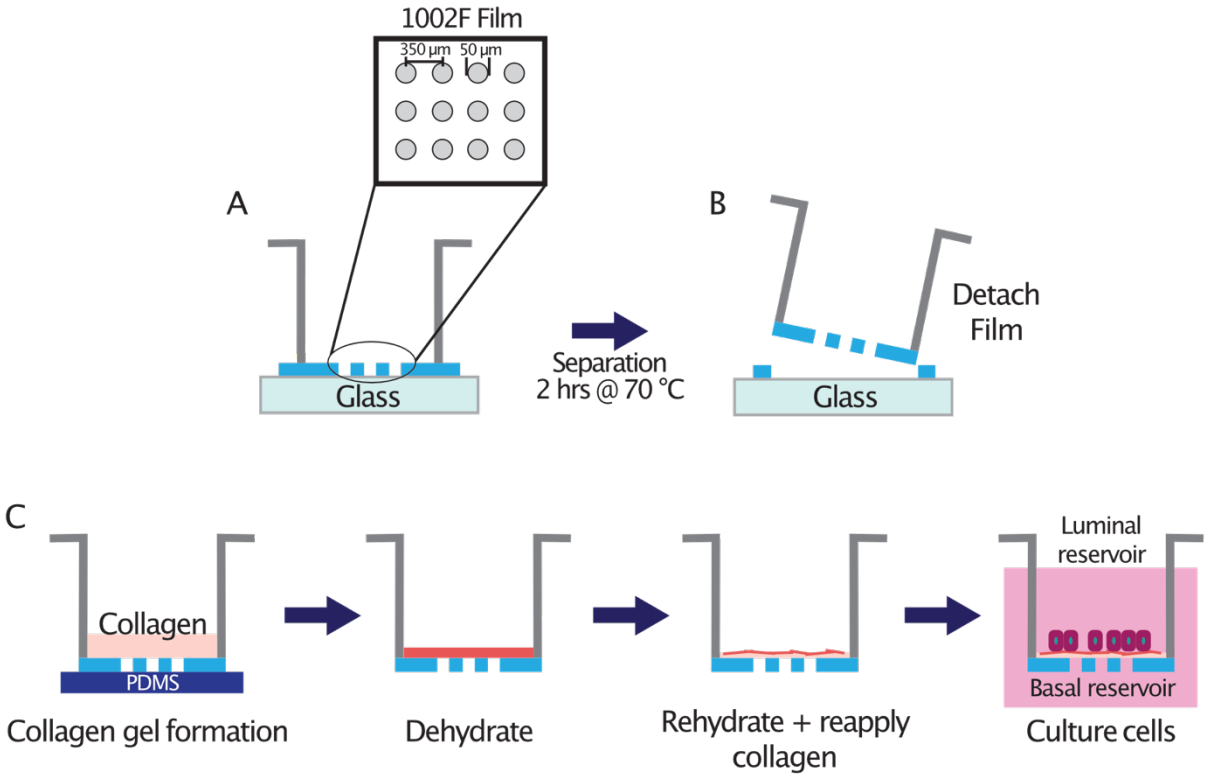

Figure 4.1 Fabrication of 2D crypt microdevice. A) 1002F-10 photoresist film is prepared on glass slide with Transwell cassette attached using 3M double-sided medical tape. B) Following incubation in water for 2 hours at 70 °C, the device is detached from glass slide. C) Preparation of compacted dehydrated collagen layer on top of the photoresist film cell culture.

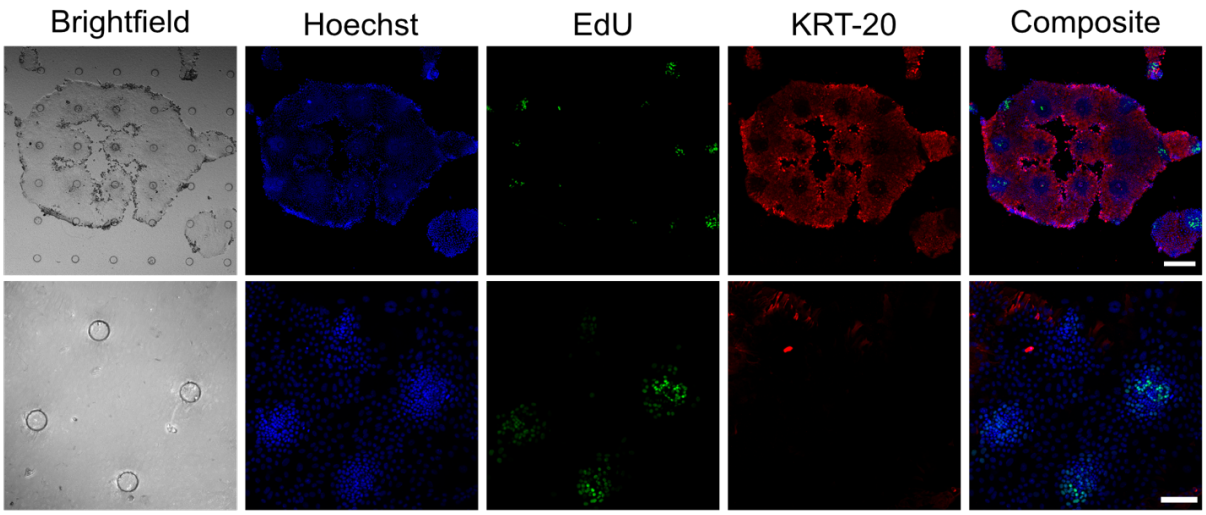

Figure 4.2 Fluorescent images of 2D crypts cultured on an array of 10 x 10 microholes, 50 µm in diameter and spaced 250 µm apart. Top row shows a 6 x 6 subset of microholes (scale bar = 250 µm), and the bottom shows a higher magnification 2 x 2 subset (scale bar = 100 µm). EM was provided to both basal and luminal reservoirs for 48 hours and then changed to EM in the basal reservoir and DM in the luminal reservoir for the following 48 hours.

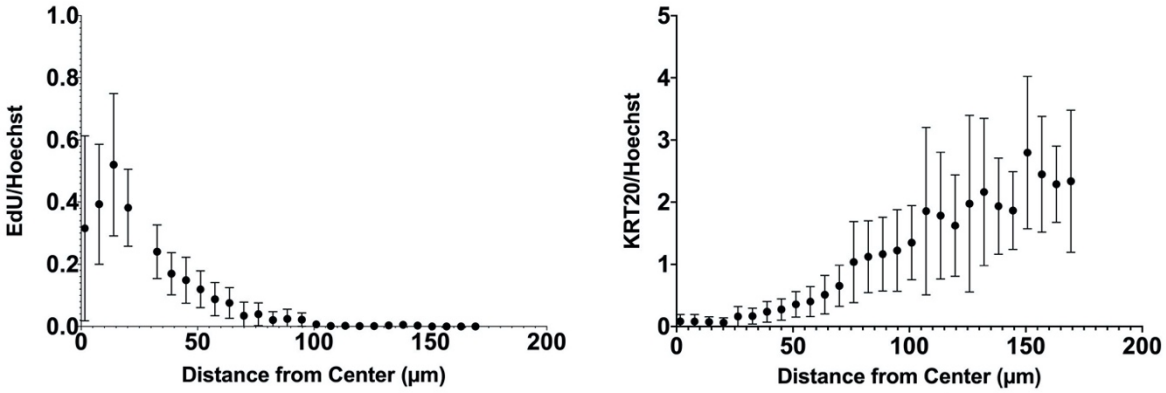

Figure 4.3 Quantification of EdU uptake for proliferative capacity and cytoplasmic protein KRT20 for differentiation status normalized to nuclear area (Hoechst). Measurements were taken in concentric circles emanating from the center of a microhole at 5 µm intervals until a distance of 175 µm, the midpoint to the nearest microhole. Values reflect the average and the error bars the standard deviation (n = 12 microholes evenly distributed across 3 devices)

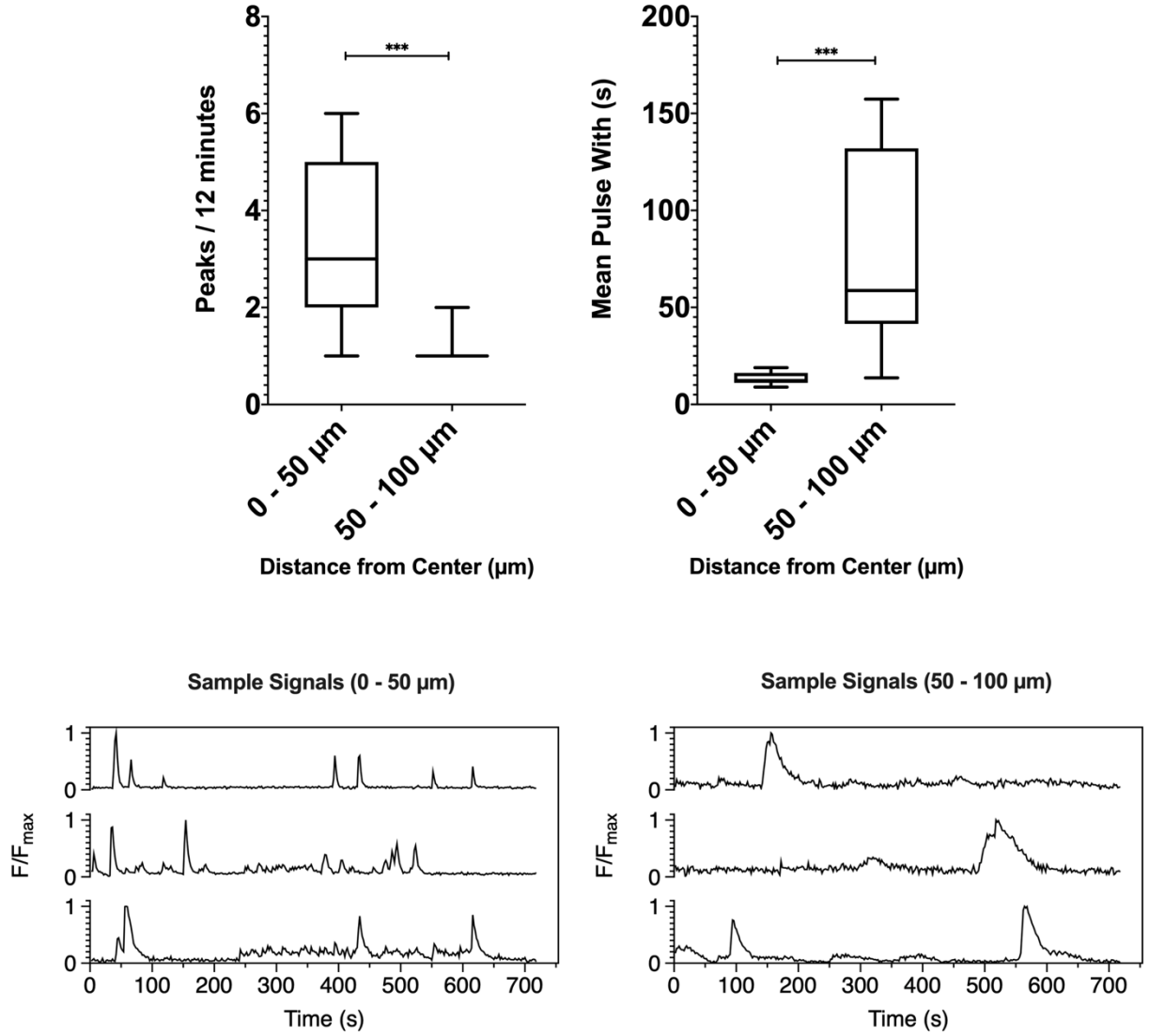

Figure 4.4 Box-and-whisker plot showing distributions of total Ca^{2+} oscillations over 12 minutes (top left) and mean pulse widths (top right) of Ca^{2+} signals group by distance from the nearest microhole center. Boxes are centered at median and extend to the 25^{th} and 75^{th} percentiles. Whiskers extend to the 5^{th} and 95^{th} percentiles. Total cell signals compared were 10 from within 50 µm of hole center and 16 cells between 50 and 100 µm from the nearest microhole center. Below are three sample signals from each category normalized to their maximum raw fluorescence. Distances for the left three signals are 10.6, 21.5, and 13.9 µm from microhole center, while distances for the right signals are 57.9, 61.5, and 89.2 µm from microhole center (top to bottom).

4.6 Tables

Table 4.1 Separation methods for 2D crypts using 1002F-10

PAA Layer	Separation Time (Hours)	Seperation Temperature (°C)	Devices Successfully Fabricated (%)*	Resulting 2D Polarization (%)**
-	15	27	19%	62%
-	48	27	37%	68%
-	2	70	87%	61%
+	15	27	87%	0%
+	2	70	94%	0%

*Prepared in batches of 16

**Following 48 hrs EM/EM and 48 hrs DM/EM

REFERENCES

1. Barker N, van de Wetering M, Clevers H, Wetering MVD, Clevers H. The intestinal stem cell. Genes & development. 2008;22:1856-1864.

2. Brittan M, Wright NA. Stem cell in gastrointestinal structure and neoplastic development. Gut. 2004;53:899-910.

3. Kosinski C, Li VSW, Chan ASY et al. Gene expression patterns of human colon tops and basal crypts and BMP antagonists as intestinal stem cell niche factors. Proceedings of the National Academy of Sciences of the United States of America. 2007;104:15418-15423.

4. Wang Y, Kim R, Hinman SS, Zwarycz B, Magness ST, Allbritton NL. Bioengineered Systems and Designer Matrices That Recapitulate the Intestinal Stem Cell Niche. Cmgh. 2018;5:440-453.e1.

5. Meran L, Baulies A, Li VSW. Intestinal Stem Cell Niche: The Extracellular Matrix and Cellular Components. Stem Cells Int. 2017;2017:7970385.

6. Pinto D, Gregorieff A, Begthel H, Clevers H. Canonical Wnt signals are essential for homeostasis of the intestinal epithelium. Genes Dev. 2003;17:1709-1713.

7. Qi Z, Li Y, Zhao B et al. BMP restricts stemness of intestinal $Lgr5^{+}$ stem cells by directly suppressing their signature genes. Nat Commun. 2017;8:13824.

8. Gjorevski N, Sachs N, Manfrin A et al. Designer matrices for intestinal stem cell and organoid culture. Nature. 2016;539:560-564.

9. Wang Y, DiSalvo M, Gunasekara DB et al. Self-renewing Monolayer of Primary Colonic or Rectal Epithelial Cells. Cmgh. 2017;4:165-182.e7.

10. Attayek PJ, Ahmad AA, Wang Y et al. In vitro polarization of colonoids to create an intestinal stem cell compartment. PLoS ONE. 2016;11:1-23.

11. Wang Y, Gunasekara DB, Attayek PJ et al. In Vitro Generation of Mouse Colon Crypts. ACS Biomaterials Science and Engineering. 2017;3:2502-2513.

12. Wang Y, Kim R, Gunasekara DB et al. Formation of Human Colonic Crypt Array by Application of Chemical Gradients Across a Shaped Epithelial Monolayer. Cmgh. 2018;5:113-130.

13. Hinman SS, Wang Y, Allbritton NL. Photopatterned Membranes and Chemical Gradients Enable Scalable Phenotypic Organization of Primary Human Colon Epithelial Models.

14. Kim R, Wang Y, Hwang SHJ et al. Formation of arrays of planar, murine, intestinal crypts possessing a stem/proliferative cell compartment and differentiated cell zone. Lab on a Chip. 2018;18:2202-2213.

15. Miyoshi H, Stappenbeck TS. In vitro expansion and genetic modification of gastrointestinal stem cells in spheroid culture. Nat Protoc. 2013;8:2471-2482.

16. DiSalvo M, Harris DM, Kantesaria S et al. Characterization of Tensioned PDMS Membranes for Imaging Cytometry on Microraft Arrays. Anal Chem. 2018;90:4792-4800.

17. Giovannucci A, Friedrich J, Gunn P et al. CaImAn: An open source tool for scalable Calcium Imaging data Analysis. bioRxiv. 2018339564.

18. Giovannucci A, Friedrich J, Deverett B, Staneva V, Chklovskii DB, Pnevmatikakis EA. CaImAn-MATLAB version 6bd51e2. GitHub

19. Zhou P, Resendez SL, Rodriguez-Romaguera J et al. Efficient and accurate extraction of in vivo calcium signals from microendoscopic video data. Elife. 2018;7

20. Zack GW, Rogers WE, Latt SA. Automatic measurement of sister chromatid exchange frequency. Journal of Histochemistry and Cytochemistry. 1977;25:741-753.

21. American PA, others. Publication manual of the American psychological association Washington. DC: American Psychological Association. 2010

22. Pai JH, Wang Y, Salazar GT et al. Photoresist with low fluorescence for bioanalytical applications. Anal Chem. 2007;79:8774-8780.

CHAPTER 5: SUMMARY AND FUTURE AIMS

5.1 Dissertation summary

This dissertation describes the development of a platform for imaging, isolation and characterization of Ca^{2+} signals in primary colon epithelium. Chapter 2 describes the initial identification of Ca^{2+} fluctuations in primary murine colon cells using a self-renewing monolayer and the Ca^{2+} indicator Cal-520 AM[1]. To accurately isolate and characterize these Ca^{2+} fluctuations, an image analysis pipeline was written in MATLAB using the CaImAn and CNMF-E image analysis packages originally develop for neuron calcium imaging[2–4]. Applying the increased throughput of the image analysis pipeline, Chapter 3 describes the impact of different extracellular stimuli on the spatial-temporal characteristics of Ca^{2+} signaling. Cultured with elevated growth factors prevalent at the base of the colon crypt, colon cells exhibited high frequency Ca^{2+} fluctuations with narrow pulse widths (>5 Ca^{2+} peaks over 12 minutes, <30 seconds mean pulse width). Under elevated differentiation factors, such as BMP and butyrate, the Ca^{2+} signaling characteristics decreased in frequency and increased in pulse width (<5 Ca^{2+} peaks over 12 minutes, >30 seconds mean pulse width). The impact of previously screened dietary compounds were also investigated, but showed a lesser dependency on Ca^{2+} signaling[1]. Finally, the properties of the extracellular matrix were investigated altering the stiffness of the scaffolding used for colon cell cultures. Cultured on a stiffer matrices (~3 GPa and 9.6 kPa, in comparison to 1.3 kPa of neutralized collagen), there was a significant decrease in frequency of

Ca^{2+} oscillations. Chapter 4 describes the improvement upon the previous work with the introduction of a microdevice capable of compartmentalizing colon cells into distinct proliferative and differentiated cell zones[5]. Imaging proliferative cell zones demonstrated cells with high frequency Ca^{2+} signals with narrow pulses while differentiated cell zones exhibited the inverse. The entirety of this work demonstrates Ca^{2+} as a signal integrator of multiple extracellular stimuli involved in the regulation of self-renewal in colon cells.

5.2 Future aims

The platform established in Chapter 2 laid out the foundations for a system for the high throughput of Ca^{2+} imaging, isolation, and characterization in primary colon epithelium. Spatial-temporal properties of the Ca^{2+} signals were quantified using basic signal analysis to measure the frequency and mean pulse width. There exist more complex signal analysis methods to perform time-frequency signal analysis such as the Fourier Transform or Wigner Distribution[6, 7]. Applying these signal analysis tools on the previously collected Ca^{2+} signals and future signals would have the potential of yielding a more detailed overview of the frequency content of these signals. This would not only improve the comparison between two cell populations but also quantifying the level of signal heterogeneity within each population.

REFERENCES

1. Wang Y, DiSalvo M, Gunasekara DB et al. Self-renewing Monolayer of Primary Colonic or Rectal Epithelial Cells. Cmgh. 2017;4:165-182.e7.

2. Giovannucci A, Friedrich J, Deverett B, Staneva V, Chklovskii DB, Pnevmatikakis EA. CaImAn-MATLAB version 6bd51e2. GitHub

3. Giovannucci A, Friedrich J, Gunn P et al. CaImAn: An open source tool for scalable Calcium Imaging data Analysis. bioRxiv. 2018339564.

4. Zhou P, Resendez SL, Rodriguez-Romaguera J et al. Efficient and accurate extraction of in vivo calcium signals from microendoscopic video data. Elife. 2018;7

5. Kim R, Wang Y, Hwang SHJ et al. Formation of arrays of planar, murine, intestinal crypts possessing a stem/proliferative cell compartment and differentiated cell zone. Lab on a Chip. 2018;18:2202-2213.

6. Lin Z. An introduction to time-frequency signal analysis. Sensor Review. 1997;17:46-53.

7. Boashash B, Ouelha S. Designing high-resolution time–frequency and time–scale distributions for the analysis and classification of non-stationary signals: a tutorial review with a comparison of features performance. Digital Signal Processing. 2018;77:120-152.